Neural Networks 27 (2012) 1–20

Contents lists available at SciVerse ScienceDirect

Neural Networks

journal homepage: www.elsevier.com/locate/neunet

Neural dynamics of saccadic and smooth pursuit eye movement coordination during visual tracking of unpredictably moving targets

Stephen Grossberg*, Krishna Srihasam, Daniel Bullock

Center for Adaptive Systems, Department of Cognitive and Neural Systems, Boston University, 677 Beacon Street, Boston, MA 02215, United States
Center of Excellence for Learning in Education, Science and Technology, Boston University, 677 Beacon Street, Boston, MA 02215, United States

ARTICLE INFO

Article history:
Received 30 December 2010
Received in revised form 14 October 2011
Accepted 20 October 2011

Keywords:
Saccade
Smooth pursuit
Eye movement
Visual tracking
MT
MST
FEF
LIP
SC
DLPN
NRTP
Cerebellum
Step-ramp paradigm

ABSTRACT

How does the brain coordinate saccadic and smooth pursuit eye movements to track objects that move in unpredictable directions and speeds? Saccadic eye movements rapidly foveate peripheral visual or auditory targets, and smooth pursuit eye movements keep the fovea pointed toward an attended moving target. Analyses of tracking data in monkeys and humans reveal systematic deviations from predictions of the simplest model of saccade–pursuit interactions, which would use no interactions other than common target selection and recruitment of shared motoneurons. Instead, saccadic and smooth pursuit movements cooperate to cancel errors of gaze position and velocity, and thus to maximize target visibility through time. How are these two systems coordinated to promote visual localization and identification of moving targets? How are saccades calibrated to correctly foveate a target despite its continued motion during the saccade? The neural model proposed here answers these questions. Modeled interactions encompass motion processing areas MT, MST, FPA, DLPN and NRTP; saccade planning and execution areas FEF, LIP, and SC; the saccadic generator in the brain stem; and the cerebellum. Simulations illustrate the model's ability to functionally explain and quantitatively simulate anatomical, neurophysiological and behavioral data about coordinated saccade–pursuit tracking.

1. Introduction

Saccadic eye movements (SACs) shift the fovea rapidly to a peripheral visual or auditory target, and smooth pursuit eye movements (SPEMs) keep the image of an attended moving target near the fovea. This paper introduces a model of how these two eye movement systems are coordinated to maintain foveation during tracking. The SAC system transforms the eccentricity of a target's retinal image relative to the fovea into the direction and amplitude of a foveating saccade (Robinson, 1964). The SPEM system can use differences between eye and target velocities to compute retinal slip, or gaze velocity error, to adjust SPEM (Krauzlis, 2005; Lisberger & Westbrook, 1985). However, retinal slip signals are insufficient for maintaining SPEM because slip is zero whenever eye velocity matches target velocity. Moreover, due to visual delays and SPEM velocity saturation, the oculomotor system cannot track by SPEM alone at high speeds. Tracking speedy targets requires "catch-up" saccades, which should be minimized because vision is degraded during saccades.

Such constraints raise many questions. How does SAC–SPEM coordination promote visual localization and visibility of moving targets? What governs decisions to initiate a saccade during smooth pursuit? Do SPEM system signals improve that decision? What happens to SPEM commands during saccades? Do SPEM commands help calibrate SAC commands to moving targets?

The SAC and SPEM systems have often been treated as separate and parallel systems interacting at only two stages: target selection and the motoneurons that control eye muscles. However, recent data imply further interactions (de Brouwer, Yuksel, Blohm, Missal, & Lefèvre, 2002; de Brouwer, Missal, Barnes, & Lefèvre, 2002; Krauzlis, 2004; Orban de Xivry & Lefèvre, 2007). In the Rashbass paradigm (Rashbass, 1961), ramp motion of a target follows an abrupt step of target position in the opposite direction. To begin tracking, monkeys sometimes begin with a catch-up saccade and sometimes show SPEM without an initial saccade. Because SAC probability depends on both step size and ramp speed (de Brouwer, Missal, & Lefèvre, 2001; de Brouwer, Yuksel et al., 2002; de Brouwer, Missal et al., 2002), target motion information supplements target position information in the control of SAC decisions.

Although prior SAC models (e.g., Brown, Bullock, & Grossberg, 2004, Dominey & Arbib, 1992, Droulez & Berthoz, 1991, Gancarz &

* Correspondence to: Center for Adaptive Systems, Boston University, 677 Beacon Street, Boston, MA 02215, United States. Tel.: +1 617 353 7858; fax: +1 617 353 7755.
E-mail address: steve@bu.edu (S. Grossberg).

0893-6080/$ – see front matter © 2011 Elsevier Ltd. All rights reserved.
doi:10.1016/j.neunet.2011.10.011

Grossberg, 1999; Girad & Berthoz, 2005; Grossberg & Kuperstein, 1986, Grossberg, Roberts, Aguilar, & Bullock, 1997, Jurgens, Becker, & Kornhuber, 1981, Optican & Quaia, 2002, Waitzman, Ma, Optican, & Wurtz, 1991) have omitted control by motion signals, such models have served as bases for many other aspects of the SAC–SPEM model presented here. Grossberg et al. (1997) predicted how visual, auditory and planned representations of target positions are aligned through learning of a multi-modal map within the superior colliculus (SC). Grossberg et al. (1997) and Brown et al. (2004) further modeled how movement gating by substantia nigra modulates release of SC motor commands. Gancarz and Grossberg (1999) proposed how several brain regions cooperate to control and adapt saccades, including how the cerebellum (CBM) corrects saccadic errors with learned context-sensitive saccadic gains. Optican et al. have proposed that the cerebellum makes on-line corrections to saccade trajectories (Lefèvre, Quaia, & Optican, 1998; Optican & Quaia, 2002; Quaia, Lefèvre, & Optican, 1999). However, as noted by Girad and Berthoz (2005, p. 223) "Their point of view is a bit extreme, as, in their models, the superior colliculus and (saccade burst generators in the brain stem) have great difficulties generating saccades . . . without the help of the cerebellum".

An important precursor of the present model is the SPEM model of Pack, Grossberg, and Mingolla (2001), which simulates human psychophysical data and monkey neurophysiological data about MST (Newsome, Wurtz, & Komatsu, 1988). As in the Robinson, Gordon, and Gordon (1986) model, Pack et al. (2001) used an efference copy of eye velocity added to the target's retinal slip to construct an internal representation of predicted target velocity that persists even if retinal slip is zero. Cerebellum-mediated gain and time-delay adaptation within a Robinson-type model were also simulated in Arakawa (2003). However, none of these models addressed SAC–SPEM interactions.

2. Model overview

The new SAC–SPEM model circuit (Fig. 1) consists of two parallel, yet interacting, processing streams. It unifies and further develops the SAC model of Grossberg et al. (1997) and Gancarz and Grossberg (1999), and the SPEM model of Pack et al. (2001). The model predicts how both types of movements are coordinated during tracking of unpredictably moving targets that give rise to movement-dependent retinal-slip error signals and positional error signals, among others.

Table 1 summarizes the neuroanatomical cell types and connections whose functional role and neurophysiological dynamics are unified within the SAC–SPEM model. Model equations and simulation details are in the Supplementary Material. The model was earlier briefly reported in Srihasam, Bullock, and Grossberg (2005, 2006a); Srihasam, Bullock, and Grossberg (2006b, 2007). A model extension simulates additional data about target selection by frontal cortex in Srihasam, Bullock, and Grossberg (2009).

The SPEM stream. How can the brain maintain SPEM during *accurate*pursuit when retinal slip signals from the tracked object are near zero? Pack, Grossberg, and Mingolla (1998); Pack et al. (2001) proposed combining target-motion, eye-speed, and background-motion signals in ventral MST (MSTv). This solution exploits computationally *complementary* properties, in MSTv and dorsal MST (MSTd) that are devoted to target tracking and optic-flow-based navigation, respectively. MST_v receives inputs from MT^-, in which *subtractive* processing via on-center off-surround directional receptive fields generates signals sensitive to the discontinuities in motion direction that arise at a moving target's boundaries. MSTd computes the *heading*, or self-motion direction, of a navigator moving through the world. It does this using *additive* processing via large directional filters that accumulate information about optic flow (Born & Tootell, 1992; Wurtz, Komatsu, Dursteler, & Yamasaki, 1990).

The model explicates how cells in MST_v can maintain an estimate of *predicted* target speed. As SPEM velocity approaches target velocity, retinal slip signals from MT^- become smaller, so MSTv cells receive less excitation. Simultaneously, background motion in the opposite direction becomes correspondingly larger. The model exploits the compensatory nature of such background whole-field motion, computed in MSTd, by adding it to those MSTv cells that compute predicted target speed in the opposite direction. In addition, corollary discharge signals that reflect current eye velocity input to the MSTv cells. Taken together, the background motion and eye velocity signals compensate for the loss of retinal slip signals as pursuit nears target speed. Support for this prediction was reported in neurophysiological experiments by Born, Groh, M m Zhao, and Lukasewycz (2000).

To incorporate these mechanisms into its SPEM circuits, the current model contains visual area MT^- and MT^+ cell types (Fig. 1; Eqs. (9) and (12)) that are selective for the direction and speed of visual stimuli that fall within their retinotopic receptive fields (Albright, 1984; Maunsell & Van Essen, 1983). The 800 model MT cells provide inputs to the model's MSTv and MSTd cells (see Eqs. (13) and (15)), which pool model MT inputs to become direction-selective and speed-sensitive, but not speed-selective. The model MSTv cells also receive background motion signals in the opposite direction, from MSTd cells, as well as corollary discharge inputs corresponding to current eye velocity from model MVN cells (Fig. 1a; see Eqs. (14) and (26)). They therefore compute an estimate of predicted target velocity that remains accurate as the growth of eye velocity toward target velocity undermines the target-induced retinal motion signals that drive model MT cells.

This model MSTv target velocity estimate drives a frontal cortical representation of desired pursuit velocity. This hypothesis is consistent with data showing that the frontal pursuit area (FPA), at the rostral bank of the arcuate sulcus, receives strong inputs from MST (Huerta, Krubitzer, & Kaas, 1987; Tian & Lynch, 1996a, 1996b). Model and real FPA cells have high direction-selectivity and speed-sensitivity, but almost no speed-selectivity (Gottlieb, Bruce, & MacAvoy, 1993; Tanaka & Lisberger, 2002b)

Model FPA cells (described in Eqs. (16)–(19)) project (Brodal, 1980a; Giolli et al., 2001) to the model NRTP (nucleus reticularis tegmenti pontis), which includes acceleration cells and velocity cells (Ono, Das, Economides, & Mustari, 2005; Ono, Das, & Mustari, 2004; Suzuki, Yamada, Hoedema, & Yee, 1999; Yamada, Suzuki, & Yee, 1996). Model NRTP velocity cells (Eq. (23)) integrate the output of model NRTP acceleration cells (Eq. (22)). The model predicts that the latter compute the difference between an excitatory target-velocity command from FPA and an inhibitory eye-velocity signal from model MVNs. The computed difference between model FPA and MVN activations estimates the eye acceleration needed to match target velocity, so both cell types enable the model NRTP to guide SPEM initiations.

Parallel to the FPA–NRTP pathway, a second pathway exists for the transmission of SPEM-related information from the cortex to the cerebellum via the pons: model MT cells project to model DLPN (dorsal lateral pontine nucleus) cells. which, in turn, project to the cerebellum (CBM); see Fig. 1a. The DLPN cells have been implicated in maintenance of SPEM (Mustari, Fuchs, & Wallman, 1988; Suzuki & Keller, 1984). In the model, the DLPN cells have speed and directional selectivities similar to MT cells, but they lack retinotopic specificity (Eq. (21)).

The saccadic stream. Reflexive saccades are drawn to sounds and visual changes. Planned saccades move the eye to intended loci, including loci that lack stimuli when an eye movement begins (White, Sparks, & Stanford, 1994). The saccadic system often executes a movement to a planned locus despite stimulation at

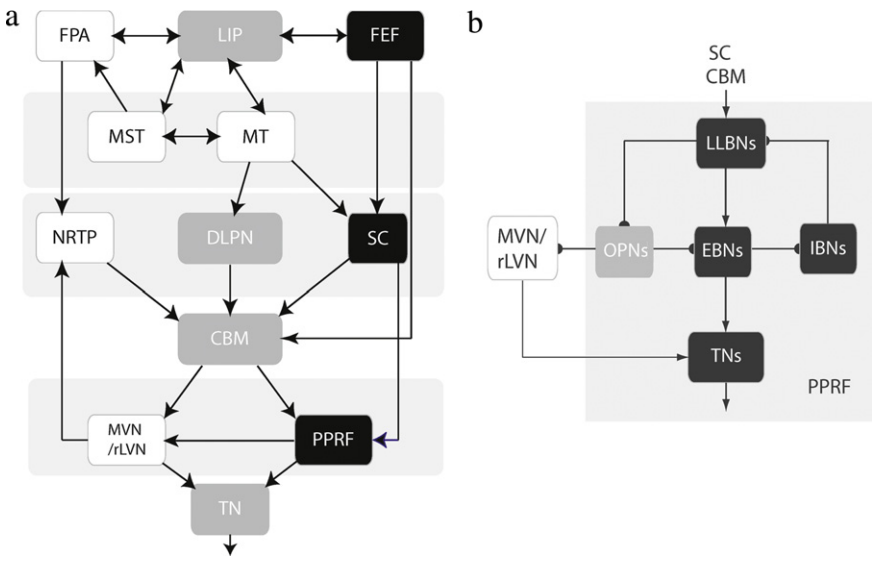

Fig. 1. (a) *Modeled interactions among brain regions implicated in oculomotor control.* Black boxes denote areas belonging to the saccadic eye movement system (SAC), white boxes the smooth pursuit eye movement system (SPEM), and gray boxes areas that belong to both systems. LIP-Lateral Intra-Parietal area; FPA-Frontal Pursuit Area; MST-Middle Superior Temporal area; MT-Middle Temporal area; FEF-Frontal Eye Fields; NRTP-Nucleus Reticularis Tegmenti Pontis; DLPN-Dorso-Lateral Pontine Nuclei; SC-Superior Colliculus; CBM-cerebellum; MVN/rLVN-Medial and Rostro-Lateral Vestibular Nuclei; PPRF-a Peri-Pontine Reticular Formation; TN-Tonic Neurons. (b) *Constituents of the saccade generator in the PPRF, and projection of omnipauser neurons to the pursuit neurons of the MVN/rLVN.* Arrows indicate excitatory connections, and semi-circles indicate inhibitory connections. OPN–Omni-Pauser Neurons; LLBN-Long-Lead Burst Neurons; EBN-Excitatory Burst Neurons; IBN-Inhibitory Burst Neurons; TN-Tonic Neurons.

Table 1
Symbols of the commonly used cells and connection weights in the simulations.

Smooth pursuit system		Saccadic system	
Symbol	Stands for	Symbol	Stands for
$v(i,j)$	Retinal velocity input at position (i,j)	r_{ij}	Retinal input at position (i,j)
m^{-}_{ijvd}	MT^{-} cells	a_{ij}	LIP cells
m^{+}_{ijvd}	MT^{+} cells	b_{ij}	SC burst layer cell
s^{V}_{d}	MST_V cells	u_{ij}	SC buildup layer cell
s^{D}_{d}	MST_D cells	u_{ff}	SC fixation cell
f^{I}_{d}	FPA input cells	f^{I}_{ij}	FEF planning layer cells
f^{S}_{d}	FPA summation cells	f^{O}_{ij}	FEF output layer cells
f^{O}_{d}	FPA output cell	f^{I}_{ff}	FEF fixation layer cell
g^{P}	Signal reflecting target choice for SPEM by a cortico-BG-thalamo– cortical loop	g^{P}	Signal reflecting target choice for SAC by a cortico-BG-thalamo–cortical loop
p^{D}_{vd}	DLPN cells	n_{ij}	Nigral cell
p^{N}_{ad}	NRTP acceleration cells	c^{F}_{ij}	Cerebellar controlled FEF input
p^{N}_{vd}	NRTP velocity cells	c^{S}_{ij}	Cerebellar controlled SC input
W^{D}_{vd}	Adaptive weights between DLPN and saccadic part of Cerebellum	W^{S}_{ij}, W^{F}_{ij}	Adaptive weights for both horizontal and vertical saccades from cerebellum for SC and FEF signal
I^{P}_{θ}	Pursuit drive along θ	I^{S}_{θ}	Saccade drive along θ
c^{P}_{d}	Cerebellar pursuit cells	l_{θ}	Long lead burst cells along θ
h_{θ}	Pursuit neurons along θ	e_{θ}	Excitatory burst cells along θ

alternative loci and detailed neural models have been developed to explain how this may occur (Brown et al., 2004; Gancarz & Grossberg, 1999; Grossberg et al., 1997). However, visually reactive, auditory, and planned saccades compete, and intense stimuli sometimes take precedence over a plan.

Because visual cues are registered in retinotopic coordinates, whereas auditory cues are registered in head-fixed coordinates, a transformation must be learned to align corresponding visual and auditory representations. Grossberg et al. (1997) modeled how burst and buildup cells in the deeper layers of SC may contribute to this learned coordinate transformation. Gancarz and Grossberg (1999) extended this model to include visual, parietal, and prefrontal cortical areas that interact to control adaptation of reactive, attentive, and planned saccades. The present unified SAC–SPEM model builds on these reports, which extensively surveyed relevant data. Below, we focus on data relevant to new SAC–SPEM interactions.

In the SAC system, retinotopically organized visual signals produce saccadic target choices in the model SC (Eqs. (30)–(45)), LIP (lateral intra-parietal area; Eq. (59)), and FEF (frontal eye fields; Eqs. (48)–(57)). Model FEF outputs input to corresponding retinotopic loci in two interacting layers of the motor error map of the model SC: activated SC *burst cells* (Eq. (30)) excite corresponding *buildup cells* (Eq. (35)).

SC outputs reach the model's cerebellum and the saccade generator circuit (Fig. 1b) in the para-median pontine reticular formation (PPRF), which contains populations of SAC- and SPEM-related cells, some of which output to the oculomotor neurons.

Outputs from cerebellar and SC stages converge at model long-lead burst neurons (LLBN). The model LLBN activity (Eq. (73)) encodes the gaze-position error and these cells excite corresponding excitatory burst neurons (EBNs). The model EBNs (Eq. (74)) project to the tonic neurons (TNs), which integrate inputs from EBNs and excite the model oculomotor neurons. The model EBNs also excite inhibitory burst neurons (IBNs), which inhibit the model LLBNs, thereby completing an internal negative feedback loop (Eq. (75)). Except during saccades, the model EBNs are inhibited by model omni-pause neurons (OPNs), whose pausing disinhibits saccades of all directions (citations in Table 1).

Shared omni-pausers. Real OPNs are located in the nucleus raphe interpositus (Buttner-Ennever & Horn, 1997; Langer & Kaneko, 1990). Model pursuit neurons (PNs) in the vestibular nuclei (MVN/rLVN) receive input from the cerebellum and project to TNs, which are shared by SAC and SPEM systems. Model PNs are weakly inhibited by, and themselves inhibit, model OPNs, also shared by both systems. About 50% of OPNs show 34% reduced activity during smooth pursuit (Missal & Keller, 2002), whereas most OPNs pause more deeply during saccades (Everling, Pare, Dorris, & Munoz, 1998, Munoz, Dorris, Par, & Everling, 2000). Thus the spontaneously active OPNs normally oppose saccades and SPEM. Shallow OPN pausing can release SPEM but not saccades, whose releases require deeper pauses.

SPEM system inhibition of SAC initiation via an MT–SC–OPN pathway. Behavioral data (simulated below) suggest an intelligent mechanism to inhibit saccade initiations during SPEM, when targets are foveal or parafoveal (i.e., when positional error (PE) is low). Pursuit-related neural activity is reliably observed in the SC: Rostral parts of SC (rSC) contain cells that respond to both SPEM and saccadic eye movements (Krauzlis, Basso, & Wurtz, 2000). As schematized in Fig. 2, area MT sends strong excitatory projections to rSC (Collins, Lyon, & Kaas, 2005; Davidson & Bender, 1991; Maioli, Domeniconi, Squatrito, & Riva Sanseverino, 1992; Spatz & Tigges, 1973), which provides the main excitatory input to OPNs (Everling et al., 1998; Gandhi & Keller, 1997; Pare & Guitton, 1994). In the model (Figs. 1 and 2a), MT foveal and para-foveal cells, which are active when pursued targets are on or near the fovea, inhibit saccades via an excitatory pathway from MT to rSC to the OPNs.

Cerebellar learning calibrates SPEM and SAC commands. Learning keeps SAC and SPEM accurate as eye muscles and other system parameters change. Cerebellar inactivation or lesion causes deficits in adapting both SAC and SPEM (Takagi, Zee, & Tamargo, 1998). Each output cell in retinotopic model FEF (Eq. (63)) and SC (Eq. (62)), each speed-sensitive cell in model DLPN (Eq. (21)), and each direction-sensitive cell in model NRTP (Eq. (23)) sends signals to the cerebellum (Thier & Ilg, 2005). These signals are modified by cerebellar learned weights. Weighted saccade-related cerebellar outputs (described in Eq. (70)) reach the model PPRF (Fig. 1a), locus of the saccade generator (Fig. 1b), and weighted pursuit-related cerebellar outputs reach the pursuit neurons (PNs) in the medial and rostro-lateral vestibular nuclei (MVN/ rLVN) of the brain stem (Fig. 1a).

3. Results: model simulations of SAC–SPEM data

Simulation 1: Threshold for catch-up saccades. During sustained pursuit of a target, the target may undergo an unexpected step change in position and velocity (de Brouwer, Yuksel et al., 2002). In general, catch-up saccades follow these unexpected steps. Catch-up saccades occur in the same direction as SPEM (forward saccades) as well as the opposite direction (reverse saccades). Parametric studies (de Brouwer, Yuksel et al., 2002; Tanaka, Yoshida, & Fukushima, 1998) show that the size and direction of the step controls the generation of the catch-up saccades. If the position step is small and in a direction opposite to target motion, catch-up saccades are generally omitted (de Brouwer, Missal et al., 2002; Missal & Keller, 2002). Thus, saccades are not reflexively generated to modest position errors during SPEM.

The modeled projection from MT to SC to the OPNs helps replicate several behaviors in the step-ramp paradigm. It is well established (de Brouwer, Missal et al., 2002; Rashbass, 1961; Van Gelder, Lebedev, & Tsui, 1995, 1997) that, by controlling the step size and the post-step target velocity, the occurrence or non-occurrence of catch-up saccades can be manipulated. Fig. 3a shows data and Fig. 3b simulations. In the top row, the target (dotted lines) first jumps and then starts moving in a direction opposite to that of the prior jump. There is a second step-ramp episode later on, with a larger jump and faster post-jump ramp. Both the first and second step-ramp combination do not elicit a saccade. Two mechanisms help achieve this: First, during near accurate pursuit (target is within $\pm 1.5^\circ$ of the fovea), the model OPNs inhibit any saccades that might be initiated due to presence of the small positional error or transient flashes (Fig. 2a). Second, as the target starts moving toward the fovea during the ramp phase after the step, the positional error, even if initially large, starts to fall. The rate of reduction in positional error depends on the velocity of the target. A target moving toward the fovea will not initiate a saccade if the target enters the para-foveal or foveal region within the latency needed to initiate a saccade (i.e., PE and RS are almost near zero). The steps in rows one and two in Fig. 3 thus elicit no saccades because the high-velocity post-step ramps bring the target near enough to the fovea to engage model rSC excitation of model OPNs before the latency to initiate a saccade. The same factors help explain observations (Rashbass, 1961; Tanaka et al., 1998) that saccades to targets moving toward the fovea are more likely to be canceled than those made to targets moving away from the fovea.

Rostral SC (rSC) contain cells that are responsive to both SPEM and SAC eye movements (Krauzlis et al., 2000). Stimulation of these cells can suppress saccades without preventing smooth pursuit movements (Basso, Krauzlis, & Wurtz, 2000). The model attributes this behavior to the differential strength of inhibition from the OPNs to the SPEM and SAC systems. Model OPNs inhibit the SAC system more strongly than the SPEM system. Because of the weaker model OPN inhibition of SPEM than SAC stages, model rSC activation during pursuit can suppress saccades without significantly inhibiting SPEM. This accords with observations that, during pursuit initiation, artificial stimulation of the rSC has only modest effects on contraversive SPEM although it suppresses ipsiversive SPEM. One possible explanation for the ipsiversive inhibition is that antidromic input from SC might reach MT (via pulvinar) and cancel the visual input present at that location. The effects of stimulation varied, such that the most rostral sites produced the most inhibition of ipsiversive pursuit (Basso et al., 2000). Such artificial stimulation was also more effective on higher pursuit speeds.

Simulation 2: Post-saccadic enhancement of pursuit motion. Tracking a moving stimulus from rest usually includes a period of smooth pursuit followed by a catch-up saccade, which brings the eye close to the position of the target. Immediately after the saccade, eye velocity closely matches target velocity even though pre-saccadic eye velocities were much lower (Lisberger, 1998). This phenomenon is called SPEM "post-saccadic enhancement". Lisberger (1998) proposed that saccades activate a switch that controls the strength of activation (or gain) of the pursuit pathway. Therefore, if pursuit is initiated without a saccade – i.e. with this switch "closed" – the pursuit system takes more time to reach target velocity. OPNs are well suited to mediate post-saccadic enhancement because model OPNs pause moderately during SPEM but deeply during saccades. We posit that, for such a gain switch to improve overall performance, it should operate within an

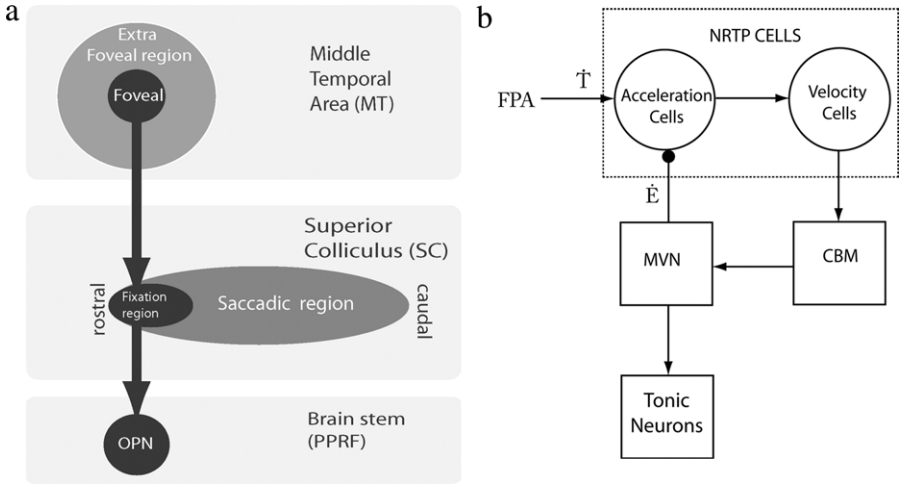

Fig. 2. (a) *Cortico-colliculo-reticular control of saccade initiation*. The figure illustrates a pathway from foveal and para-foveal cells in cortical area MT to the rostral pole of the SC and then to the OPNs in the PPRF. Effective tracking causes MT foveal cells to become active. This, in turn, activates fixation cells present in the rostral SC. Such SC cells excite OPNs, which can inhibit saccade initiation or suspend on-going saccades. (b) *Sustained pursuit and integration of acceleration signals in NRTP*. In the model, sustained pursuit is possible even if successful SPEM drives the retinal slip rate to zero, because pursuit is guided by a cortical estimate of target velocity, not by retinal slip as such. To update the SPEM velocity command, the model utilizes an internal negative feedback loop to compute the difference between the cortical estimate of target velocity ($\dot{T}$) and the currently commanded eye velocity ($\dot{E}$), which strongly depends on learned cerebellar inputs to the vestibular nuclei. The computed difference between two velocity estimates yields a desired acceleration signal, which must be integrated to form a sustained command for desired SPEM velocity. The model NRTP performs differencing and integration to create both acceleration and velocity cells, and with the NRTP's receipt of high-level velocity-related signals from the FPA (frontal pursuit area) and low-level velocity-related signals from the MVN (medial vestibular nucleus). The model NRTP acceleration cells thus act as a comparator between the estimated target velocity and estimated eye velocity. The output from these cells is integrated by the model NRTP's velocity neurons.

internal negative feedback loop (Fig. 2b) which prevents the eye velocity command that results from enhanced gain in the pursuit pathway from increasing much beyond the current estimate of target velocity.

What anatomical substrates realize these mechanisms? The NRTP contains gaze acceleration and gaze velocity cells (Ono et al., 2005, 2004; Suzuki et al., 1999; Suzuki, Yamada, & Yee, 2003; Yamada et al., 1996) that act as velocity-comparison and velocity integrator cells (Fig. 2b). Model FPA cells output to the NRTP of the brain stem (Brodal, 1980a, 1980b; Giolli et al., 2001). Model vestibular nuclei (MVN/rLVN), whose efferents control pursuit eye movements, also send collateral signals to NRTP (Torigoe, Blanks, & Precht, 1986). These efference copies are extra-retinal signals of the current eye velocity. NRTP acceleration cells subtract this eye velocity estimate from the current target velocity estimate generated by the FPA output cells. NRTP velocity cells then integrate the activity of NRTP acceleration cells. Any mismatch between the current eye velocity and estimated target velocity generates a compensatory signal that pushes the current eye velocity toward the estimated target velocity. Thus post-saccadic enhancement operates within a circuit that matches eye velocity to predicted target velocity.

Fig. 4 compares the results of model simulations (right column) with data (left column, from (Lisberger, 1998)). Panels 4a–4d show traces of eye velocity, and target and eye positions, for a single target step combined with different motion onset times. In panel 4a, there is no delay between the initial target step and subsequent smooth motion. As the delay between the initial step and the onset of subsequent smooth target motion increases to 50, 100, and 150 ms in 4b–4d, the pursuit system has decreasing time to estimate the target velocity before saccade initiation. In the model, insufficient time leads to a velocity underestimate, and this causes reduced post-saccadic eye velocity—visible in both simulations and data. While the traces (Fig. 4c and d, right side) in simulations look qualitatively similar, the simulations show a lower post-saccadic enhancement due to noise in the system. Longer latencies between target step and motion onset cause hypometric saccades because, as explained below, saccades are pre-adapted to compensate for estimated target motion. This is corrected by a subsequent saccade as seen in 4c and 4d. However, the interval between successive saccades is long enough (Kalesnykas & Hallett, 1994, 1996) that the motion system can accurately estimate target velocity. At the end of the second, correcting, saccade (cf., Figs. 4 and 4c, d), the pursuit eye velocity can exceed target velocity. But, the proposed negative feedback from model rLVN/MVN to model NRTP acceleration neurons (Fig. 2b) limits any such velocity overshoots. Once the SPEM velocity exceeds estimated target velocity, input to the NRTP velocity integrators terminates, and the opposite direction is activated. Such an internal negative feedback also helps explain small steady-state oscillations around the target velocity (cf., Arakawa, 2003; Robinson et al., 1986).

Simulation 3: MT modulates pursuit gain after a saccade. In adults, *pursuit gain* (the ratio of eye velocity to target velocity) is usually around 1.0. However, modest deviations above or below unity are often observed in SPEM after saccades, and such departures compensate for modest foveation errors remaining after the prior saccade. If the saccade overshoots, but by too little to evoke a corrective saccade, a SPEM gain less than one allows the target to catch up to the moving line of gaze. If the saccade undershoots, a SPEM gain above unity allows the line of gaze to catch the target, without a catch-up saccade. Such behavior avoids the loss of visibility that would be entailed if small gaze position errors always elicited corrective saccades. In the model, such "saccadic chatter" is avoided via two complementary mechanisms. First, the foveation error must exceed a positive threshold to elicit a saccade. Second, overshoots and undershoots affect the size of the population recruited in area MT, and this population response scales the pursuit gain in a way that compensates for overshoots and undershoots (Fig. 5g). Since model MT receptive fields do not cross the vertical meridian, an overshoot, accurate saccade, or undershoot, respectively, can cause recruitment of (relatively) low, medium, and high numbers of active MT cells in the controlling hemisphere. These recruitment levels lead to corresponding pursuit gains, of $1-\varepsilon$, ~ 1, and $1+\varepsilon$, where ε is a small fraction of 1. See Fig. 1 for a simulation illustrating the latter property.

Simulation 4: Gap effect in saccade latency. If during pursuit, the target blinks or disappears for a short duration and then re-appears at a different location, the saccade latency is less than

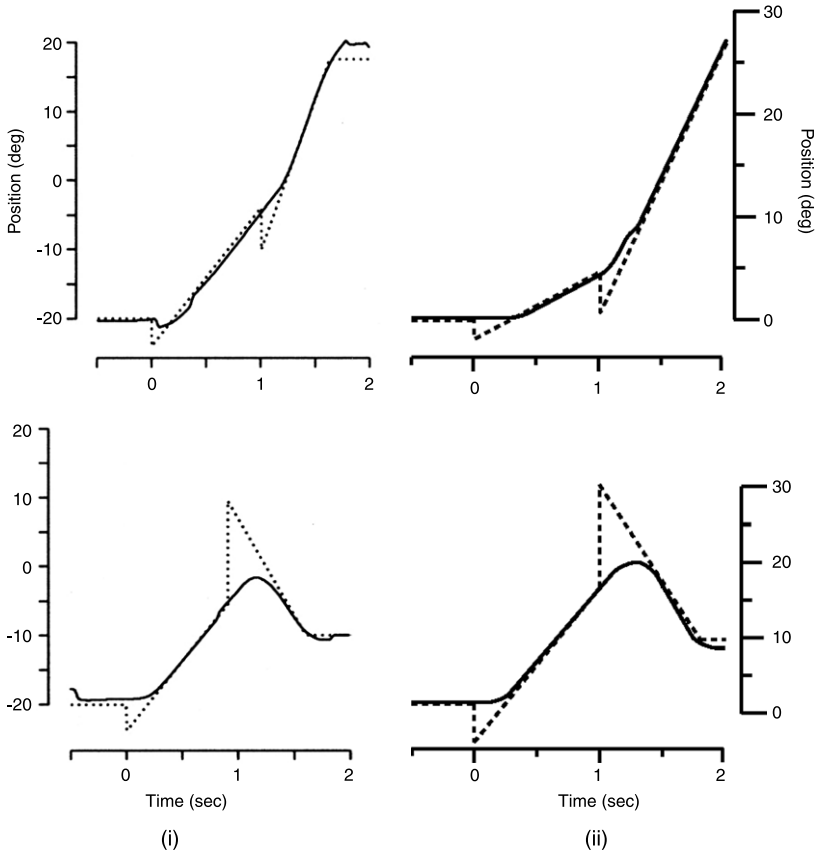

Fig. 3. *Step-ramp paradigms illustrate dual control of saccade decisions: Data and simulations*. The left column (a) shows data from humans exposed to step-ramp paradigms. The right column (b) shows model simulation results that replicate performance in these experimental paradigms. For both simulations (top and bottom panels), the target initially jumped 3° left and started moving rightwards with a speed of 20°/s. For the top panel, At $t = 1$ s, the target again jumped by 5° left and started moving rightwards with a speed of 30°/s. For the bottom panel, the target again jumped by 5° right and started moving leftwards with a speed of 30°/s. Each panel shows horizontal target position (dotted trace) and gaze-position (continuous trace) versus time. Once foveation of a target is achieved, a step change in either position or speed, or both, unexpectedly occurs. The top row shows, near $t = 1$ s, a backward step in position, i.e., in a direction opposite to the prior target motion and SPEM. That target step is followed by continued target motion in the original direction, but at increased speed. This combination does not induce a catch-up saccade. The bottom row shows a step along the direction of prior target motion, followed by a reversal of target motion direction. This combination also induces no catch-up saccade. Thus, even in the presence of a significant gaze-position error, a saccade is usually omitted when the target's motion is reducing the error and is therefore likely to render the saccade unnecessary.
Source: Reprinted, with permission, from de Brouwer, Yuksel et al. (2002).

the saccade latency of a saccade to a target that remained visible until its jump (Krauzlis & Miles, 1996a; Tanaka et al., 1998), much like the reduction in saccade latency to stationary targets in gap tasks (Klingstone & Klein, 1991; Tam & Stelmach, 1993), in which a foveated fixation point disappears prior to peripheral target presentation.

In the model, gap and blink affects on saccade latency depend on inhibition of the saccadic output channel at two stages: the SC and the EBN (see Fig. 1). Saccade-generating cells in the caudal SC of the model (Fig. 2a) receive inhibition from two sets of cells assumed to be excited while a foveated stimulus is on: fixation-activated cells in rostral SC (rSC) and fixation-activated cells in the substantia nigra pars reticulata (SNr). During gap or blink intervals, there is no visual input to such fixation-activated cells, so inhibition to caudal SC from both rSC and SNr drops, and this enables shorter saccadic latencies once the target appears and excites SC buildup and burst cells. Moreover, EBNs in the saccade generator are normally inhibited by OPNs that, in turn, are excited by fixation-activated rSC cells. Upon disappearance of a fixation stimulus, this inhibition decreases and promotes shorter latencies, as simulated in Fig. 6a.

Simulation 5: SPEM direction affects the size of saccade. Consider a catch-up saccade during pursuit of a moving target. To compensate for target motion, the amplitude of a catch-up saccade typically differs from that of a saccade to a static target at the same initial eccentricity (de Brouwer, Missal et al., 2002; Eggert, Guan, Bayer, & Buttner, 2005; Guan, Eggert, Bayer, & Buttner, 2005; Missal, Coimbra, Lefèvre, & Olivier, 2002). After establishing that SC firing specified *equivalent* amplitudes for two saccades of *unequal* amplitudes made to a moving or stationary target, Keller, Gandhi, and Weir (1996) hypothesized that the trans-SC path (SC to PPRF, Fig. 1b), which programs a saccade solely on the basis of the pre-saccadic gaze-position error, is assisted by another path that corrects the programmed saccade by using information about target speed.

In the model, speed-tuned extra-foveal MT cells project to the cerebellum via DLPN (Fig. 1a), and errors trigger cerebellar learning of the correct gain for relating saccadic size increments to target velocity. The pre-saccadic gaze error causes activation of the vector error map in SC. This initiates a saccade of a particular size. In addition, velocity information from MT extra-foveal cells is processed by the cerebellum to correct saccadic size: Saccades to targets with centrifugal motion are stretched and saccades to targets with centripetal motion are shortened.

Fig. 7 schematizes these two pathways, and Fig. 6b compares data (Guan et al., 2005) with model simulations for two step-ramp stimuli. In one, the initial step is larger, but the ramp has negative slope, corresponding to target motion back toward the initial line of gaze. In the second (superimposed on the same plot to facilitate comparison), the initial step is smaller, but the ramp is positive, corresponding to continued motion away from the initial line of gaze (Fig. 6b: i). After 200 ms, the two ramp

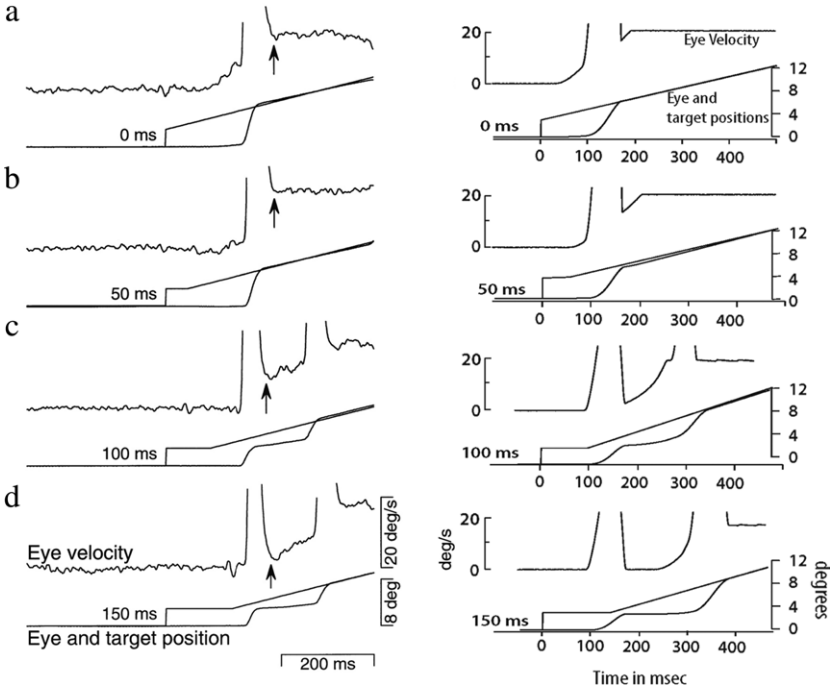

Fig. 4. *Saccadic enhancement of the rate of change of pursuit velocity*. The time it takes to make a transition from one SPEM velocity to another depends on saccadic activity. The rate of change of SPEM velocity during a saccade is higher than during a non-saccadic period. It has been postulated that a switch that is partly controlled by the saccadic pathway modulates the SPEM command. In the model, this interaction arises because OPNs used by the saccadic system also inhibit brain stem neurons that carry the SPEM velocity command (see Fig. 1(b)). Each of panels (a)–(d) in the left column show an eye velocity trace (truncated at the high velocities achieved during saccades) above target position and eye position traces for a monkey performing a variant of the step-ramp paradigm. Although the step in position was always 4° and the change in ramp slope (target velocity) was always 20°/s, in panel (a) the target step onset and the ramp motion onset coincided, in panel (b) the ramp motion was delayed for 50 ms, in panel (c), for 100 ms and in panel (d), for 150 ms. In panels (c) and (d), the SPEM velocity after the first saccade is notably less than the target velocity. The right column shows that model simulation results closely match the data.
Source: Reprinted, with permission, from Lisberger (1998).

target motions reach the same point in space and cross over. The saccade to the larger step is smaller than the saccade to the smaller step, contrary to what one would expect if the saccade amplitudes reflected only the initial steps, but illustrative of velocity-based compensation. Similar compensation is visible in simulations of the full model (Fig. 6b: ii), but not in a model lacking learned cerebellar compensation (Fig. 6b: iii).

Simulation 6: SPEM direction affects the latency of saccade. Saccades to target steps in the same direction as the preceding pursuit have shorter latencies than those to target steps in the opposite direction in both gap and non-gap trials (Krauzlis & Miles, 1996b; Tanaka et al., 1998). Because a gap makes no difference, and both steps are away from the fovea, differential OPN excitation should not be a factor. The longer time needed for the moving eye to reverse its direction is partly biomechanical: an interval of force integration is needed to slow the eye to a zero velocity. In the model, a distinct component of latency arises from the same mechanisms of velocity-dependent saccade pre-compensation just discussed. The left column of Fig. 8a shows the behavioral data (Tanaka et al., 1998) and right column shows the simulation. The target jumps at the same time and by the same amount in either of the directions (forward or backward), but in data and model the saccades made to steps in the opposite direction of SPEM take longer to initiate. The latency difference is already apparent at the EBN stage (Figs. 1b and 8c). This reflects the LLBN signals (Fig. 8b) in the two cases, which differ because of velocity-dependent pre-compensation via the DLPN–CBM–LLBN pathway (Fig. 1). Data from Tanaka et al. (1998) show a 36 ms latency difference between forward and backward saccades. Our simulations generated a 25 ms latency difference. The extra 10 ms difference might be due to biomechanics, or switching of attention from one hemisphere to other. Human psycho-physical data (Van Donkelaar & Drew, 2002) show that attention during pursuit is either on the pursued target or ahead of it. Forward (backward) saccades use attentional resources of the same (opposite) hemisphere.

Simulated activations for all major neuron types: Fig. 9 illustrates model neural activations along the saccadic (right column) and SPEM (left column) pathways that generated the simulated gaze behaviors shown in the right column of Fig. 4c. The bottom row shows neuron activations that send movement commands to tonic neurons: SPEM system rLVN/MVN neurons (Fig. 9j) and SAC system EBNs (Fig. 9t). Because the SPEM command (Fig. 9j) is zero before the first EBN burst (Fig. 9t), but grows significantly during that burst, the SPEM velocity is zero before the first saccade, yet significantly positive as soon as the first saccade ends. Fig. 9r shows that the OPNs, which tonically inhibit both command pathways, pause during SPEM or SAC, but much more deeply during SAC. This deep pause enables the EBNs to burst, but also permits rapid growth of the SPEM velocity command during SAC, and thus "post-saccadic enhancement".

To illustrate this interaction, the OPN trace from Fig. 9r reappears as a dashed trace in Fig. 9f. The continuous trace shows a model NRTP acceleration cell. The panel below it shows a model NRTP velocity cell. The minimum value of OPN activity (during SAC) slightly leads the maximal acceleration toward the peak sustained SPEM velocity. Also model MST_v activity (Fig. 9a) persists during sustained SPEM despite the fact that target-related model MST_d activity (Fig. 9b, dotted trace) wanes as eye velocity matches target velocity, and thereby cancels target-related retinal slip, even as background slip (Fig. 9b, solid trace) opposite to target direction is maintained.

4. Discussion and conclusions

This article describes a neural model of how SPEM and SAC systems interact during a variety of oculomotor tasks. The model

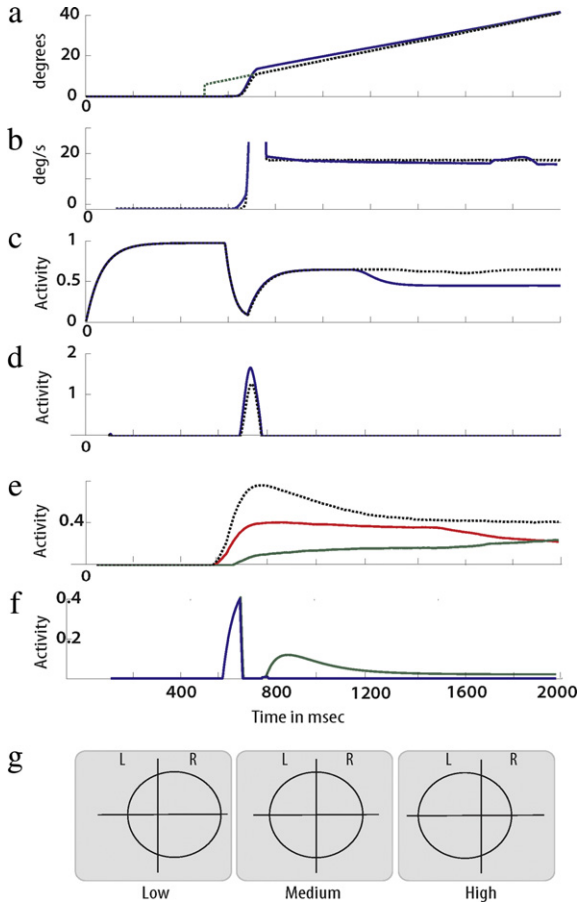

Fig. 5. *Pursuit gain drops transiently after a saccadic overshoot.* Panel (a) shows simulated eye position for an accurate saccade (dashed black trace) and a saccade that overshoots the target (solid blue trace). When catch-up saccades made in the direction of target motion overshoot by modest amplitudes, the system (real and simulated) does not compensate by a reverse saccade, which would reduce visibility. Instead, it compensates by reducing SPEM velocity (panel (b), solid blue trace), and thus *pursuit gain*, the ratio of eye to target velocity. This relative slowing of the eye allows the target to catch up. The interval from $t = 800$ to 1700 shows the period in which the pursuit gain is reduced, with foveation occurring at $t = 1700$. In the model, gain reduction cannot be explained by the depth of OPN pausing (panel (c)), nor by the saccade-related activity in SC (panel (d)). But a clear difference between the two episodes is apparent in two sites, MSTv (panel (e); the dashed line is the activity of MSTv cell in the opposite hemisphere in the overshoot episode) and DLPN (panel (f)), that are excited by area MT. Panel (g): in area MT, an overshoot, an accurate saccade, and an undershoot respectively entail recruitment of (relatively) low, medium, and high numbers of area MT cells in the controlling hemisphere. These recruitment levels lead to corresponding pursuit gains, in the immediate postsaccadic interval, of $1-\varepsilon$, 1, and $1+\varepsilon$, where ε is a small fraction of 1. For these simulations, the initial target jump was always 4° right and target ramp speed was always at 20°/s in rightward direction.

proposes a unified explanation of many recent single neuron recordings and key behavioral trends observed under various experimental conditions (e.g.,de Brouwer et al., 2001; de Brouwer, Yuksel et al., 2002; de Brouwer, Missal et al., 2002; Krauzlis & Miles, 1996a, 1996b; Missal et al., 2002; Missal & Keller, 2002; Tanaka et al., 1998).

The model provides mathematically explicit answers to fundamental questions: what happens to smooth pursuit commands when a saccade is initiated to a moving target? The two systems operate in parallel during the saccade. Parallel operation uses the model's representation of target velocity which persists despite loss or degradation of target-related visual inputs, such as occurs during a catch-up saccade, brief occlusions of a tracked target, or as a consequence of successful SPEM, which zeros target motion, but not background motion, in the retinal frame. Such parallel operation, combined with the shared omnipauser stage, enables the model to explain post-saccadic enhancement of SPEM.

How can saccades to moving targets be accurate? The model offers a two-part answer. Parallel operation means that the saccade does not have to pre-compensate for target motion to the (large) extent that it would if the SPEM system were quiescent during the saccade. However, because of underestimates of target velocity within the SPEM system in the often brief pre-saccadic interval, or because of velocity saturation in the SPEM system, occasions regularly arise in which a catch-up saccade will be inaccurate (before learning) *despite* parallel operation of SPEM. The resulting post-saccadic foveation errors enable learning in the model cerebellum to use target velocity information to improve the metrics of catch-up saccades.

Recent behavioral data (Schreiber, Missal, & Lefèvre, 2006) show that under certain circumstances, such as when there is asynchrony between position and motion signals, a saccade can change its direction during execution and is double-peaked. We believe that the curvature of these double-peaked saccades in the above-mentioned paper is due to competitive execution of two successive saccade plans. As mentioned in the model overview, there are two inputs that trigger a saccade in our model: positional error and retinal slip. If the planned saccadic directions of both triggers do not agree (e.g., if they do not command the same direction), the model can generate a curved, double peaked saccade as seen in the data (Schreiber et al., 2006). The first part of the double-peaked saccade will be along the direction of positional error (PE Saccade) and the second part will be along the direction of positional error generated by retinal slip (RS Saccade). Since the pathways for these two inputs are different (PE via SC and RS via DLPN) in the model, the execution of the first plan does not negate the presence of the second. However, there is competition at the level of LLBNs. So, as soon as the activation of LLBN cells executing the PE saccade fall below the activity of the second group of cells representing the RS saccade plan, the second plan starts to move the eye and the saccade curves.

Because saccades do degrade vision, it is also important to understand what mechanisms collectively reduce saccadic "chatter" (excessive corrective saccades) during near-accurate tracking. Two model mechanisms cooperate to achieve this result. Small foveation errors activate a pathway that includes MT, rostral SC and the OPNs, whose excitation inhibits saccades. Another pathway, from MT to the pons, enables a transient reduction of SPEM gain after an overshooting saccade. This reduces the need for back-tracking saccades by slowing SPEM and allowing the target to catch up with the moving line of gaze.

Two other pertinent models have recently appeared. The oculomotor control system (OCS) model (Lee & Galiana, 2005) guides two cameras mounted on a robotic head to track a moving target. The model was tested for ramp and sinusoidal trajectories, but not for a wide range of step-ramp stimuli (Rashbass, 1961). The OCS model exhibits saccade size adaptation for moving targets. Notably, it uses slip information to correct the amplitude of saccades made to moving targets. The model estimates the corrective displacement by multiplying the target's pre-saccadic retinal slip by a constant (proportional to saccadic duration) and adds it to the retinal-position error to program a compensatory saccade. However, these corrections must be quite large, because the OCS model's saccadic system shuts off its smooth pursuit system during a saccadic suppression phase. Thus it cannot benefit from parallel operation of SPEM during its saccades. This causes an increase in gaze position and velocity errors after saccades (Fig. 4 in Lee & Galiana, 2005). Data of Lisberger (1998) strongly suggest that the two systems do operate in parallel, as in our model. The OCS model's authors acknowledge its inability to explain post-saccadic enhancement of eye velocity.

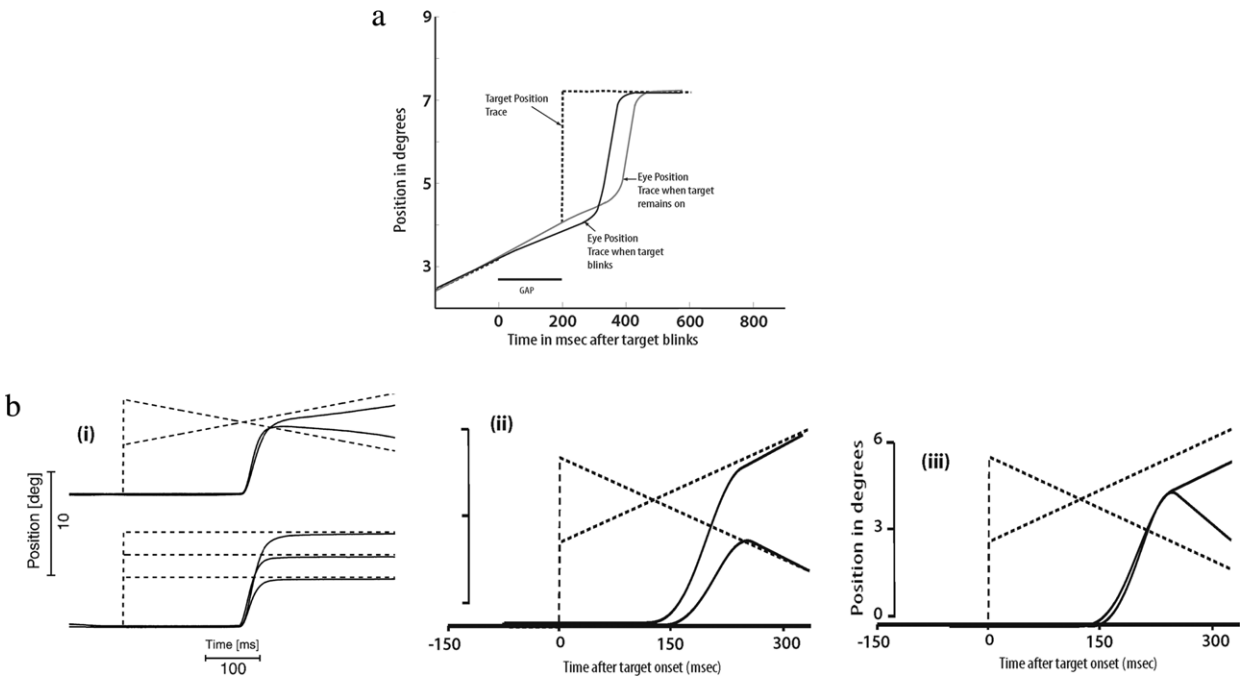

Fig. 6. (a) *Simulated gap effect on saccadic latency*. Blinking or masking of a smoothly pursued target before a step of target position reduces the latency of the saccade generated immediately after the step. This effect can be seen irrespective of prior target motion, i.e., if a stationary or moving foveated light is switched off before the onset of a stepped target, saccadic latencies are shorter than if the foveated target had remained on. The figure plots positions versus time and superposes results from two simulations. The dotted black line shows the target presentation trace, which begins with a ramp and may or may not have a gap, in display of the ramp motion, just before the step to a new, final position. For the case with a gap, the simulated eye position (solid black trace) shows a reduction in pursuit velocity during the gap, followed by a short-latency saccade in response to reappearance of the target at the new location. When there is no gap, the eye position (thick gray trace) shows a long-latency saccade in response to the step. To simulate these conditions, ramp velocity of 20°/s in rightward direction was used. Target was blinked for around 100 ms after which, the target appears and remains stationary at 3° ahead of the current target position. Because of the random noise being added in the model, no two eye position traces will be exactly the same even with exactly the same parameters. (b) *Data and model simulations showing that catch-up saccades compensate for target velocity*. Amplitudes of catch-up saccades pre-compensate for a target's expected displacement due to its continued motion during the saccade. The first panel (i) shows stimuli and eye movement data from Guan et al. (2005). The second (panel (ii)) and third (panel (iii)) panels show simulation results with and without cerebellar compensation. In the two simulation trials, a large or a medium step occurs. The large step (6°) is followed by motion back toward the initial position 71 (speed is 20°/s, toward the fixation point). The small step (3°) is followed by further motion away from the initial position (speed is 20°/s, away from fixation point). That the saccade in response to the larger step is notably smaller than the saccade in response to the small step in the middle panel (panel (ii)) shows that the full model system (like the real system of panel (i)) is making the compensation for target velocity that is needed to improve the likelihood of having the eye fall wherever the moving target will be at the end of the saccade. The lower panel (panel (iii)) shows that the model without the cerebellar component is unable to use target-motion information to pre-compensate.

Without specifying a computational model, Blohm, Missal, and Lefèvre (2005) proposed that a subsystem may integrate SPEM velocity commands to compute SPEM-based gaze displacements needed for correct targeting of memory-guided saccades. The "smooth double-step" paradigm (McKenzie & Lisberger, 1986) analyzed by Blohm et al. (2005) uses a brief flash to specify a second saccadic target while the subject is still actively pursuing the first. Once the pursued target disappears, the subject must make a saccade to the remembered location of the briefly flashed target. Since SPEM continues up to the time of the saccade to the remembered target, that target's initially recorded retinotopic position is inaccurate by an amount equal to the integral of the post-flash SPEM velocity; i.e., the net eye-displacement since the flash. Data (Blohm, Missal, & Lefèvre, 2003; Blohm et al., 2005; Gellman & Fletcher, 1992; McKenzie & Lisberger, 1986) show a range of memory-saccade latencies, with short latency saccades inaccurate, but longer latency saccades accurate. Blohm et al. (2005) posit that only longer latency saccades incorporate post-flash SPEM displacement. Thus, their conceptual model's saccadic pathway gets a smooth eye velocity displacement signal (SED_{est}) generated by an eye velocity integration (EV) mechanism. Once the second target flashes, the EV mechanism starts integrating. Since the integration process is assumed to be slow, longer latencies give the saccade generator access to better SED_{est} values, and so the ensuing saccades are accurate. The conceptual model has no specific mechanism for triggering a saccade. It uses experimental data directly as its basis for a distribution of saccadic latencies.

It seems premature to assume that the system solves problems of the type posed by such double-step experiments in the manner proposed. For example, suppose that subjects instead adopt the strategy of immediately recoding the flashed target's location from retinotopic to head-centered coordinates (cf., Grossberg & Kuperstein, 1989). Then the need to compute the intervening SPEM displacement would be obviated (if the head remains fixed, as it must if SPEM integration would be sufficient). Instead, the subject could merely compare eye position at the end of SPEM with the stored target position to compute the correct saccade vector. If this account is correct, then fast-inaccurate saccades need a different explanation than lack of access to a slowly arriving displacement signal. One possibility is that the fast-inaccurate saccades actually reflect an average between two computed saccade vectors, one based on a head-centered representation and one on a not-yet-faded retinotopic representation. Such a possibility warrants examination, because in other double-flash paradigms, the probability of saccadic averaging is a declining function of saccade latency (Chou, Sommer, & Schiller, 1999). Resolving such issues is beyond the scope of the present model.

Most of target tracking in the real world happens on textured backgrounds that are either moving or stationary. Previous studies on humans and monkeys show that the pursuit eye movement system has trouble differentiating target motion from background (Humans: Yee, Daniels, Jones, Baloh, & Honrubia, 1983; van den Berg & Collewijn, 1986; Lindner, Schwarz, & Ilg, 2001;

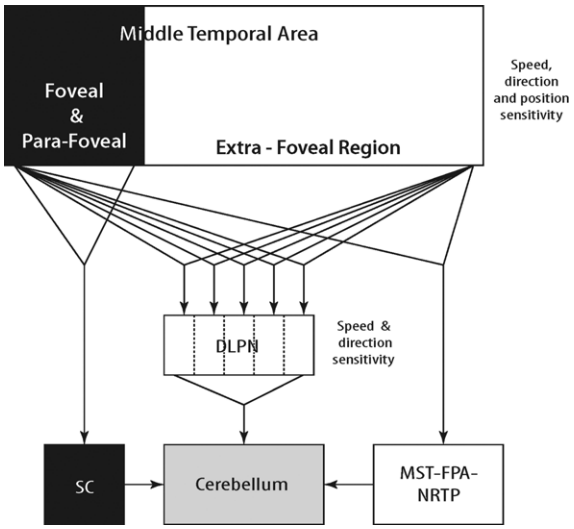

Fig. 7. *Adjusting the amplitudes of saccades made to moving targets*. Cortical area MT helps inhibit small saccades and calibrate catch-up saccades. Direction-sensitive MT cells representing the foveal and parafoveal space send projections to rostral SC, thereby inhibiting small saccades. Extra-foveal MT neurons that are speed, direction and retinal-position specific project to cerebellum via DLPN (dorso-lateral pontine nucleus) cells that are speed and direction (but not retinal-position) selective. This motion vector information helps the saccadic system compensate for the target motion that occurs during a saccade by modulating the size of that saccade.

Masson, Proteau, L, & Mestre, 1995; Niemann & Hoffmann, 1997; Monkeys: Born et al., 2000; Keller & Khan, 1986; Kimmig, Miles, & Schwarz, 1992; Kodaka, Miura, Suehiro, Takemura, & Kawano, 2003; Mohrmann & Thier, 1995).

Introducing background motion during different phases of pursuit causes different results. Background motion during pursuit maintenance (van den Berg & Collewijn, 1986; Mohrmann & Thier, 1995; Niemann & Hoffmann, 1997; Yee et al., 1983) increases the speed of pursuit (or gain) if the introduced motion is along the direction of the target motion ("same direction effect"). On the other hand, background motion causes two different effects on pursuit initiation based on the type of trial: ramp trial or step-ramp trial. In ramp trials (Masson et al., 1995), introduced motion along the direction of the target causes same direction effects. But in a step-ramp trial, if the background motion in the direction opposite to target motion, it increases the gain ("opposite direction effect"). So, if the background motion is foveo-fugal (moving away from the fovea) it increases the gain of pursuit, and if the background motion is foveo-petal it reduces the gain, irrespective of the state of the pursuit.

Earlier model from our group (Pack et al., 2001) assumed that a stationary background causes a retinal sweep signal in the opposite direction of target pursuit. This signal compensates for loss of visual information during accurate pursuit in the maintenance phase. This model also assumes that pursuit signal ("p" in Eq. (1) of Pack et al., 2001) is zero during fixation on a stationary target. But a moving background causes an involuntary eye movement called opto-kinetic nystagmus (OKN), which is evolutionarily old. It has been hypothesized that an internal pursuit signal is needed to suppress this response and maintain fixation (Leigh & Zee, 1999). In Pack et al. (2001), competition between pursuit channels encoding opposite directions of eye movement allows model cells to suppress stimuli that would normally trigger a disruptive movement to track the retinal motion of the background. Pack et al. (2001) argued that this mechanism may be sufficient to suppress at least the cortical portion of the OKN response. Directionally opponent interactions also occur in the current expanded model, as in Eq. (77). A more thorough examination and modeling of the genesis of this suppressing signal is beyond the scope of this paper.

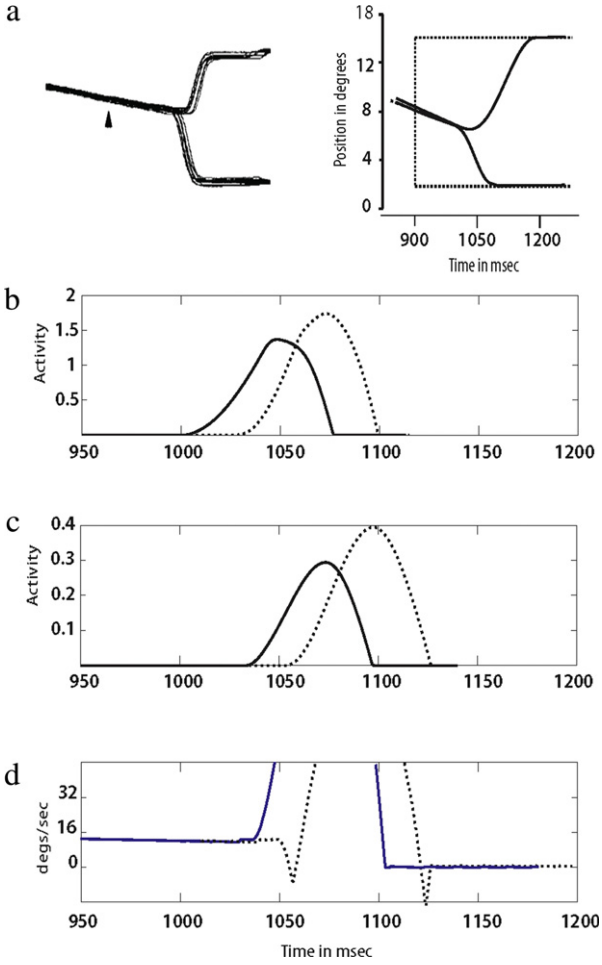

Fig. 8. *Saccadic latency is affected by the direction of the target jump*. Saccades to target jumps along the direction of pursuit have smaller latencies than those to jumps opposite to the direction of pursuit. Panel (a): Left column shows data from Tanaka et al. (1998). There is a 36 ms difference between the saccadic initiation times. The right column shows results of simulations (ramp speed before step jump was 20°/s leftwards. A step jump of 6° either direction was introduced. The target remains stationary afterward), which yielded roughly a 25 ms difference between saccadic initiation times for saccades to jumps along, versus in the opposite direction of, target motion. The dashed trace shows the target position and solid traces show eye position. Panels (b)–(d) compare the activations of model LLBNs, EBNs and eye velocity traces during forward (target jump along the direction of motion) and backward saccades (jump direction is opposite to target motion) respectively. Dotted lines represent the traces for the backward saccade and thick lines illustrate the traces for the forward saccade. These panels show activity for the duration between 50 and 300 ms after the target jump. This time period was highlighted to exemplify the differential pontine neuronal activations that lead to forward and backward saccades. Model LLBNs and EBNs show earlier activations for the forward saccade than for the backward saccade.

Acknowledgments

Authorship is in rotated alphabetical order. DB, SG and KS were supported in part by CELEST, an NSF Science of Learning Center grant (SBE-0354378). SG was also supported in part by the SyNAPSE program of DARPA (HRL subcontract HR0011-09-C-0001) and by the Office of Naval Research (ONR N00014-01-1-0624).

Appendix. Model equations and parameters

The model is designed to capture key aspects of the processing of visual and motor signals in saccadic and smooth pursuit areas. The model simulates cell responses in such areas (Fig. 1) through the use of nonlinear differential equations based on the classical membrane equation (Grossberg, 1973, 1982; Hodgkin, 1964). The

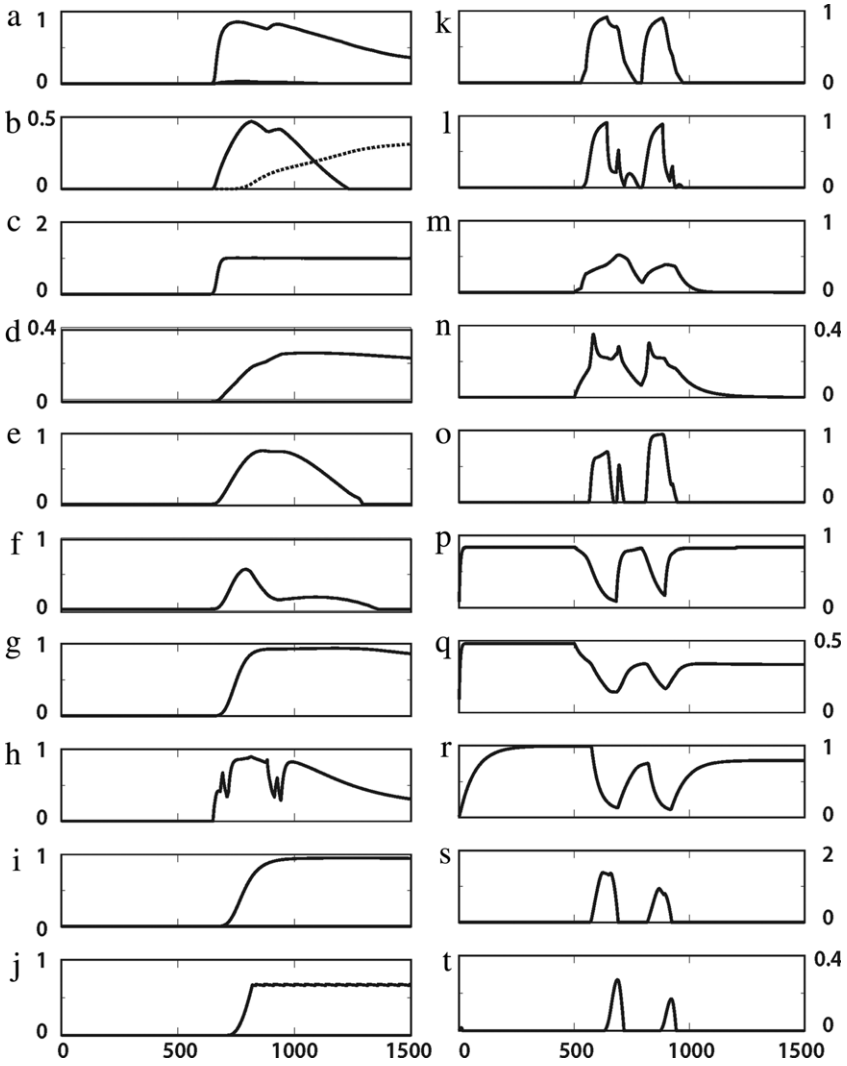

Fig. 9. *Simulated activities of all the main model cell types.* The right column shows SAC system activations, the left column SPEM system activations. These simulated neural activities generated the simulated gaze behavior shown in panel (c) in the right column of Fig. 5. The target stepped 4° rightward along the horizontal axis, and then, after a 150 ms delay, continued smooth rightward motion at a speed of 20°/sec. For those left-column areas where cell types are direction-selective, the plots show only activities of cells whose preferred direction aligned with the rightward target motion direction. (a): MST_v cell; (b): MST_d cell activities for target-motion direction (dashed trace) and for background motion direction (solid trace); (c): FPA_i cell; (d): FPA_o cell; (e): FPA_s cell; (f): $NRTP_a$ cell, with dashed overlay of OPN activity trace from (r); (g): $NRTP_v$ cell; (h): DLPN cell; (i) CBM cell; (j): MVN cell. Right column: panels (k), (l), (m), (n) and (o), respectively, shows activities of FEF_v, FEF_m, LIP, SC_{burst}, $SC_{buildup}$ cells whose receptive fields are centered at a 4° eccentricity. Panels (p), (q) and (r), respectively, represent activities of model FEF_{fix}, SC_{fix} and OPN cells. Panels (s) and (t) show activities of LLBNs and EBNs that generate rightward eye motion.

Table 2
Symbols that are common to both SAC and SPEM systems.

Symbol	Represents
θ	Directions along which the muscle can move the eye
d	Directions along which the target can move
t_θ	Tonic neuron activity along θ
o	Omnipauser neuron activity
Ψ	Eye position

system of equations was numerically integrated using the fourth order Runge–Kutta method, with a fixed step size of 0.001 s. Tables 2 and 3 summarize model variable names and parameters.

Visual inputs. Each visual input to the smooth pursuit circuit is a vector field that describes the speed of the motion at each point (x, y). The values of x and y are each constrained to be between $[-1, 1]$ which is mapped to $[-60°, 60°]$ in visual space. The velocities $v(x, y)$ are constrained between the values $[0, 1]$. The target is a square block of length and width r moving in any one of the eight cardinal directions in the visual field. The center of the object is given by (x_0, y_0) and its speed is v_0. The retinal image velocity, $v'(x, y)$, is calculated as the difference between object speed and the eye speed at that point. Target visibility is controlled by two variables T_{on} and T_{off}, which specify the on and off times of the target in the simulation. Fixation offset is marked by T_{fix} set equal to 500.

MT cell. The cells representing the input for the smooth pursuit circuit are modeled after cells found in the middle temporal area (MT). MT cells have speed and direction tuning (Maunsell & Van Essen, 1983). Two different types of cells have been observed in MT. One type, MT^- cells, respond vigorously to small stimuli moving in their receptive field at a particular speed and in a particular direction. The second type, MT^+ cells, respond to large stimulus sizes. There is a large MT projection to MST. MST also has two major cell types. Cells in ventral MST (MST_V) show direction-sensitive modulation to object motion (Tanaka, Sugita, Moriya, & Saito, 1993). Cells found in dorsal MST (MST_d) respond to large field stimulus motion. These target tracking and navigation cells are computed using complementary subtractive vs additive operations (Grossberg, 2000; Grossberg, Mingolla, & Pack, 1999; Pack et al., 2001).

Table 3
Model neurons and their empirically determined connectivity and physiological properties.

Connection in model	Functional interpretation	References
LIP to FEF, FEF to LIP	Saccadic target selection	(Barbas & Mesulam, 1981; Huerta et al., 1987)
FEF to SC, SC to FEF	Planned saccade information	(Fries, 1984; Huerta et al., 1987; Leichnetz, 1981; Leichnetz et al., 1981)
LIP to SC, SC to LIP	Saccadic target priming information	(Lynch et al., 1985)
FEF to PPRF	Motor command for saccade generation	(Huerta et al., 1987; Leichnetz et al., 1984)
SC to PPRF	Motor command for saccade generation	(Harting, 1977; May & Porter, 1992; Scudder et al., 1996a, 1996b)
SC to CBM	Saccadic command for fine tuning	
SC to cNRTP		(Harting, 1977)
cNRTP to Vermis		(Thielert & Thier, 1993; Yamada & Noda, 1987)
MT to MST, MST to MT	Target velocity signal is constructed	(Tusa & Ungerleider, 1988)
MST to DLPN	Target and background speed and direction input is projected	(Glickstein et al., 1980; Mustari et al., 1988; Ono et al., 2004; Suzuki & Keller, 1984)
MST to FPA	Direction and speed sensitive of target data	(Churchland & Lisberger, 2005; Maioli et al., 1992; Tian & Lynch, 1997, 1996a, 1996b; Tusa & Ungerleider, 1988)
FPA to rNRTP	Direction sensitive target input reach eye acceleration cells in rNRTP.	(Suzuki et al., 1999, 2003; Yamada et al., 1996)
DLPN to CBM	Target and background speed and direction input is transferred.	(Mustari et al., 1988; Ono et al., 2005, 2004)
DLPN to Vermis		(Thielert & Thier, 1993; Yamada & Noda, 1987)
DLPN to VPF		(Nagao et al., 1997)
rNRTP to CBM (floccular complex)	Specific target data is transferred to CBM	(Giolli et al., 2001; Suzuki et al., 1999; Yamada et al., 1996)
CBM(floccular complex) to MVN/vLVN	Smooth pursuit Signal	(Lisberger et al., 1994; Roy & Cullen, 2003)
MVN/vLVN to NRTP	Eye velocity feedback signal	(Torigoe et al., 1986)
LIP to MT/MST	Saccadic target selection information is passed to SPEM system	(Andersen et al., 1990; Blatt et al., 1990)
MT to SC	Foveo-fugal speed sensitive input to rostral fixation cells	(Fries, 1984; Maioli et al., 1992; Spatz & Tigges, 1973)

We simulated 100 model MT cells for each of the eight cardinal directions (800 cells total). Each cell had a preferred speed and direction. The receptive field (i, j) was constrained to be between [-1, 1]. The speed tuning of a cell at position (i, j) is defined by a Gaussian function, G^v_{ijxy}, centered on a preferred speed v_{ij}. The direction tuning was also a Gaussian function, G^d_{ij}, centered on the preferred direction d_{ij}. Noise is added as input to every cell in the model. Term Δ_N represents a random number between 0 and 1 picked from a uniform distribution. The total amount of noise being added to any cell is determined by multiplying a tenth of the current activation of the cell with Δ_N.

Each MT cell has a receptive field size dictated by the eccentricity of the cell from the fovea. Cells that are farther from the fovea have bigger receptive fields in keeping with the cortical magnification factor. The width of each receptive field, W_{ij}, as a function of the cell's position in retinotopic space, is given by

$$W_{ij} = \frac{25}{0.91(i^2 + j^2)^{0.5} + 1.0}. \tag{1}$$

Each MT cell has a preferred direction which is selected at random from any of the eight cardinal directions. It also has a preferred velocity, v_{ij}, chosen from the distribution $e^{-Q(v-0.5)^2}$. Only inputs matching these directional preferences activate the cell. For each MT cell, the total response to a motion stimulus was characterized in terms of center–surround inputs to that MT cell. The on-center response, α^+_{ij}, of the receptive field to a visual target depends on the presence of three factors: the position (x, y) of the target within its receptive field, the velocity $(v(x, y))$ of the target near the preferred velocity (v_{ij}), and the direction (d) of the target along or near the preferred direction (d_{ij}) of the cell, namely:

$$\alpha^+_{ij}(v_{ij}, d_{ij}) = \sum_{x,y} G^{cp}_{ijxy} G^v_{ijxy} G^d_{ij}. \tag{2}$$

In (2), G^{cp}_{ijxy} represents the position sensitivity of the cell. It decreases as the target moves away from the center of the MT response field by:

$$G^{cp}_{ijxy} = e^{-W_{ij}[(i-x)^2 + (j-y)^2]}. \tag{3}$$

Similar to position sensitivity, G^v_{ijxy} represents the velocity tuning of the MT cell. This term reaches its maximal value if the velocity of the target $(v(x, y))$ is the same as the preferred velocity (v_{ij}) of the cell:

$$G^v_{ijxy} = e^{-G_1(v_{ij} - v(x,y))^2}. \tag{4}$$

MT cell activity also depends on the direction (d) of target motion relative to the cells preferred direction (d_{ij}). This term can be calculated as:

$$G^d_{ij} = e^{-G_2(d_{ij} - d)^2}. \tag{5}$$

Parameters G_1 and G_2, in Eqs. (4) and (5) equal 10 and 6, respectively.

MT cells also receive input from surround regions α^-_{ij}, chosen to be five times the size of the on-centers:

$$\alpha^-_{ij}(v_{ij}, d_{ij}) = \sum_{x,y} G^{sp}_{ijxy} G^v_{ijxy} G^d_{ij}. \tag{6}$$

In (6), the position sensitivity (G^{sp}_{ijxy}) is calculated as

$$G^{sp}_{ijxy} = e^{-\frac{W_{ij}[(i-x)^2 + (j-y)^2]}{25}}, \tag{7}$$

and G^v_{ijxy} and G^d_{ij} are defined as in Eqs. (4) and (5).

The model computes MT^+ cell activities by *adding* the surround to the center component, and MT^- cells by *subtracting* the surround from the center component.

Subtractive cells (MT^-). A model MT^- cell input is given by:

$$\beta^-_{ij}(v_{ij}, d_{ij}) = \left[\alpha^+_{ij}(v_{ij}, d_{ij}) - \alpha^-_{ij}(v_{ij}, d_{ij})\right]^+, \tag{8}$$

and its activation dynamics are described by:

$$\frac{dm^-_{ijvd}}{dt} = -m^-_{ijvd} + (1 - m^-_{ijvd}) \times \left(\beta^-_{ij}(v_{ij}, d_{ij})(1 + [s^-_d]^+) + \sum_{ab} a_{ab} W_{abij}\right) - (1 + m^-_{ijvd}) \sum_{e \neq d} s^-_e + 0.1 m^-_{ijvd} \Delta_N. \quad (9)$$

Apart from the directional tuned input ($\beta^-_{ij}(v_{ij}, d_{ij})$), model MT$^-$ also receives top-down modulatory excitatory input from the MST$_V$ cell (term s^-_d) having the same directional preference as the MT$^-$ cell and from LIP (term $\sum_{ab} a_{ab} W_{abij}$). It is also inhibited by MST$_V$ cells tuned to different directions (term $\sum_{e \neq d} s^-_e$) as part of the top-down attentional MST$_V$ feedback. Term $0.1 m^-_{ijvd} \Delta_N$ in Eq. (9) represents the noise that is added to the system to break symmetry. Term $\sum_{ab} a_{ab} W_{abij}$ in Eqs. (9) and (12) represents an excitatory input from an LIP neuron with a retinotopic receptive field (W_{abij}) that is in register with that of the recipient MT neuron:

$$W_{abij} = \begin{cases} 1 & \text{if } a - \delta/2 < i < a + \delta/2 \quad \text{and} \\ & b - \delta/2 < j < b + \delta/2 \\ 0 & \text{otherwise.} \end{cases} \quad (10)$$

In (10), δ represents the diameter of LIP neurons response field. Thus, W_{abij} enables a saccadic decision to enhance MT and MST processing of a selected target.

Additive cells (MT$^+$). A model MT$^+$ cell's net center–surround input is given by:

$$\beta^+_{ij}(v_{ij}, d_{ij}) = \alpha^+_{ij}(v_{ij}, d_{ij}) + \alpha^-_{ij}(v_{ij}, d_{ij}), \quad (11)$$

and its activation dynamics are described by

$$\frac{dm^+_{ijvd}}{dt} = -m^+_{ijvd} + (1 - m^+_{ijvd}) \times \left(\beta^+_{ij}(v_{ij}, d_{ij})(1 + [s^+_d]^+) + \sum_{ab} a_{ab} W_{abij}\right) - (1 + m^+_{ijvd}) \sum_{e \neq d} s^+_e + 0.1 m^+_{ijvd} \Delta_N. \quad (12)$$

MT$^+$ cells also receive excitatory input from MST cells, but from the dorsal sub-region (term s^+_d) as compared to the ventral sub-region for MT$^-$ cells. They also receive an excitatory input from LIP (term $\sum_{ab} a_{ab} W_{abij}$), as well as inhibition ($-\sum_{e \neq d} s^+_e$), from MT$^-$ recipient MST$_D$ cells coding for non-matching directions.

The top-down inputs from MST to MT are consistent with data (Seidemann & Newsome, 1999; Treue & Maunsell, 1999) indicating that MT cell activity is modulated by top-down attention. This top-down modulatory on-center, off-surround circuit has been shown capable of focusing attention while also stabilizing learning in the network (Carpenter & Grossberg, 1993; Grossberg, 1980, 2003).

MST cells. Inputs from model MT cells with varying speed selectivities but similar directional preferences are pooled by direction-tuned, speed-sensitive cells in the model MST. MT$^-$ cells project to MST$_V$ and MT$^+$ cells project to MST$_D$. The MST$_D$ activities are symbolized by s^+_d, and the MST$_V$ activities by s^-_d, where subscript d indicates the cell's direction preference and D indicates direction anti-parallel to cell's preferred direction. Direction "d" takes the values 0°, 45°, 90°, 135°, 180°, 225°, 270°, 315°.

Target tracking cells (MST$_V$). Target tracking cells in MST (s^-_d) calculate an estimate of predicted target velocity during pursuit. Their input comes from retinal sources (from MT) and extra-retinal sources (via a corollary discharge) and thus can provide a reliable estimate of target velocity even during sustained pursuit. The activities of the small-field MST$_V$ cells are given by:

$$\frac{ds^-_d}{dt} = -s^-_d + (1 - s^-_d)\left[2.5 \sum_{ij} [m^-_{ijvd}]^+ v_{ij} + 5.5[s^+_D]^+ + 2(k_d - k_D)\right]^+ - 75 \sum_{e \neq d} s^-_e + 0.1 s^-_d \Delta_N. \quad (13)$$

In (13), term $\sum_{ij} m^-_{ijvd} v_{ij}$ gives an estimate of the average velocity computed by the MT$^-$ cells having the same direction preference. Other sources of excitatory input come from the large-field MST$_D$ cell having an opposite direction to this MST$_V$ cell (term s^+_D), and via corollary discharge ($k_d - k_D$) (see Pack et al. (2001)) and noise ($0.1 s^-_d \Delta_N$). There is also mutual inhibition between the MST$_V$ cells coding other directions (term $-75 \sum_{e \neq d} s^V_e$).

Input from MST$_D$ cells having an opposite directional preference to MST$_V$ cells that represents a pursued target are excited by the background counter-motion generated by SPEM. Such excitation helps MST$_V$ to better compute predicted target velocity when visual motion inputs decrease from MT$^-$ cells to MST$_V$ cells during successful pursuit. In Eq. (13), k_d is a corollary discharge, or efference copy, from the pursuit neurons of the vestibular nucleus that fire when the eye moves in direction d (see Eq. (26) below), and k_D is the corollary discharge from pursuit neurons that fire when the eye moves in the direction D that is opposite to d. Term k_d is calculated as a mix of the two nearest orthogonal signals θ and $\theta + 90°$ to d from the values 0°, 90°, 180° and 270°:

$$k_d = \sqrt{h^2_\theta + h^2_{\theta+90}}. \quad (14)$$

These corollary discharge signals, which grow as the eye velocity grows to match the velocity of the SPEM target, can also compensate for the reduction of small-field visual motion signals that attend any successful SPEM. The result is that *MST$_V$* cells can provide a reliable estimate of predicted target velocity throughout a SPEM episode, namely before SPEM onset, during SPEM acceleration, and during steady-state matching of eye to target velocity.

Motion opponency of the efference signals ($k_d - k_D$) in Eq. (14) supports this type of activity profile. During SPEM onset, $[k_d - k_D]$ is zero. Once the eye starts to move, $[k_d - k_D]$ becomes excitatory for MST$_V$ cells aligned along direction of target motion and inhibitory for the MST$_V$ cells in the opposite direction. This pattern is reversed for MST$_D$ cells as seen in the Eq. (15).

Navigation cells (MST$_D$). MST$_D$ cell get input from the large receptive field MT$^+$ cells having same directional preference, and so is sensitive to coherent background motion. The activities of the large-field MST$_D$ cells are given by:

$$\frac{ds^+_d}{dt} = -s^+_d + (1 - s^+_d)\left[0.1 \sum_{ij} [m^+_{ijvd}]^+ + 5.5[s^-_d]^+ + 2(k_D - k_d)\right]^+ - 15 \sum_{e \neq d} s^+_e + 0.1 s^+_d \Delta_N. \quad (15)$$

The excitatory input to MST$_D$ cells comes from three sources: MT$^+$ cells ($\sum_{ij} m^+_{ijvd}$) having the same directional preference as the model MST$_D$ cell, the MST$_V$ cell (s^-_d) having the same directional preference, and via corollary discharge ($k_D - k_d$). There is mutual inhibition between the MST$_D$ cells coding other directions (term $-15 \sum_{e \neq d} s^+_e$). Note that the corollary discharge input ($k_D - k_d$) to the cell is the opposite of the corollary discharge to MST$_V$ cell (see Eq. (13)). This opponency ensures that, during sustained pursuit,

the activity of MST_D cells tuned to background motion direction remains bounded and does not affect the current pursuit dynamics.

FPA cells: The frontal pursuit area (FPA) is considered to be the first area where a sensory-to-motor transformation of SPEM signals takes place. The model FPA contains three cell types that model cells reported in literature (Tanaka & Lisberger, 2002a):

Winner-Take-All cells (WTA). WTA cells receive input from target-tracking cells of MST and convey this information to the target-selective FPA vector averaging cells. Their activity, f_d^I, obeys:

$$\frac{df_d^I}{dt} = -2f_d^I + (1 - f_d^I)\left(50[s_d^-]^+ + 10f_d^R\right) - 10\sum_{e\neq d} f_e^I + 0.1f_d^I\Delta_N. \tag{16}$$

By (16), these cells are excited by MST_V cells (term $50[s_d^-]^+$) having the same directional preference, and by self-excitatory interneurons (term $10f_d^R$). There is mutual inhibition among input cells with different direction preferences (term $-10\sum_{e\neq d} f_e^I$). The excitatory interneurons within the input layer support self-sustaining activity:

$$\frac{df_d^R}{dt} = -f_d^R + (1 - f_d^R)[f_d^I]^+ + 0.1f_d^R\Delta_N. \tag{17}$$

Vector summation cells. Vector summation cells receive input from the navigation cells of MST and provide additional acceleration during pursuit initiation. These activities obey:

$$\frac{df_d^S}{dt} = -f_d^S + (1 - f_d^S)15[s_d^+]^+ - (1 + f_d^S) \times \sum_{e\neq d} f_e^S + 0.1f_d^S\Delta_N. \tag{18}$$

Summation cell activities (f_d^S) are excited by MST_D cells of the corresponding direction (term $15s_d^+$), and have low mutual inhibition (term $-\sum_{e\neq d} f_e^S$). This inhibition enables two stimulus directions to be simultaneously active and enables vector averaging to occur before target selection.

Vector averaging output cells. Model vector averaging cells perform the role of target selection cells in the SPEM system. These cells interact with basal ganglia via thalamus and help decide the target stimulus among many distractors. These activities obey:

$$\frac{df_d^O}{dt} = -10f_d^O + (1 - f_d^O)(15[f_d^I]^+ + [f_d^S]^+ + 15\mu^d + 1.5[g^P - 0.5]^+) - 25(1 + f_d^O) \times \sum_{e\neq d} f_e^O + 0.1f_d^O\Delta_N. \tag{19}$$

FPA output activities (f_d^O) are excited by FPA input cells (term $15f_d^I$) and summation cells (f_d^S) having the same direction preference, by electrical stimulation (μ^d), and by a cortico-thalamic decision signal ($[g^P - 0.5]^+$). The cortico-thalamic decision signal helps in target selection when more than one stimulus is present in the environment. The output cells receive strong inhibitory input from output cells with different direction preferences (term $-25\sum_{e\neq d} f_e^O$). If several FPA input cells are active at the same time, indicating more than one moving target, the output cells show a reduced response due to this inhibitory process.

Model FPA output cells carry the estimate of target velocity. FPA WTA cells (see Eq. (16)) receive direct inputs from MST_V cells which estimate the target velocity. This activity is sustained even during target blink via the self-excitatory interneuron. During single stimulus tracking, FPA output cells carry the target velocity estimate from MST_V to NRTP. When multiple stimuli are present, FPA input cells hold the representations of all stimuli until FPA output cells decide the target among the distractors. Once FPA output cells select a target for a future SPEM, the activity of FPA input cells representing the distractor starts decaying.

Decision signal (g^P). Onset of the gating signal g^p in (19) occurs once the total activity reaches 0.5. Then, BG-Thal sends a nonspecific signal that boosts the activity of all the FPA averaging cells. Mutual inhibition helps choose the winner. Thus, this interaction results in a choice that is controlled by a cortico-basal ganglia-thalamocortical loop (Basso & Wurtz, 2002; Brown et al., 2004). Its value is calculated as:

$$\frac{dg^P}{dt} = -0.2g^P + (1 - g^P)\sum_d [f_d^O - 0.33]^+ + 0.1g^P\Delta_N. \tag{20}$$

In (20), g^P is activated by a thresholded input from FPA output cells (f_d^O). When g^P exceeds 0.5 (see Eq. (19)), the FPA output cell with maximal activity is chosen as the target and the competition is silenced via strong mutual inhibition.

Pontine nuclei. Pontine nuclei act as way stations for the SPEM information transfer from cortex to cerebellum. We have modeled two important pontine nuclei, namely DLPN and NRTP.

DLPN cells. DLPN cells have large receptive fields covering almost the whole contra-lateral visual field and have directional preferences and speed selectivities similar to MT cells. There is no topographic arrangement of cells in DLPN. The activities of DLPN cells obey:

$$\frac{dp_{vd}^D}{dt} = -p_{vd}^D + 0.1(1 - p_{vd}^D)\sum_{ij}[m_{ijvd}^-]^+ - 100(1 - p_{vd}^D) \times \sum_{\substack{e\neq d\\ f\neq v}} p_{fe}^D g^P + 0.1p_{vd}^D\Delta_N. \tag{21}$$

By (21), DLPN cells receive convergent excitatory inputs from all MT^- cells of the same speed and direction (term m_{ijvd}^-). Mutual inhibition among DLPN cells (term $-100\sum_{\substack{e\neq d\\ f\neq v}} p_{fe}^D$) enables only those neurons whose velocity tuning is close to that of the target velocity to remain active. Therefore, model DLPN cells output an approximate estimate of target velocity without regard to its specific retinotopic locus. This approximate estimate provides drive to the initial eye acceleration (see Eq. (24)) and helps the cerebellum make corrections to the amplitudes of saccades made to moving targets (see Eq. (70)).

NRTP cells. Two types of pursuit-related cells have been observed in NRTP: acceleration cells and velocity cells (see Simulation 2 and Fig. 2b). We predict that the acceleration cells act within an internal negative feedback loop to compute the difference between estimated target velocity and eye velocity. The velocity cells integrate acceleration cell output.

NRTP acceleration cells: NRTP acceleration cell output acts as a mismatch detector between the estimates of target and eye velocities. The activities of these cells obey the equation:

$$\frac{dp_{ad}^N}{dt} = -p_{ad}^N + 45(1 - p_{ad}^N)\left[f_d^O - k_d\right]^+ - 50\sum_{e\neq d} p_{ae}^N + 0.1p_{ad}^N\Delta_N. \tag{22}$$

The acceleration cells (p_{ad}^N) are excited by the difference between the FPA output that estimates target velocity, and k_d, the vestibular nuclei (rLVN/ MVN, see Eq. (14)) output that controls, and thus estimates, eye velocity. There is also mutual inhibition between different NRTP acceleration cells ($-50\sum_{e\neq d} p_{ae}^N$).

NRTP velocity cells: The activities of these cells follow the equation:

$$\frac{dp^N_{vd}}{dt} = -0.4p^N_{vd} + 40(1 - p^N_{vd})[p^N_{ad}]^+ + 0.1p^N_{vd}\Delta_N. \tag{23}$$

Acceleration cell activity p^N_{ad} in Eq. (22) is the only excitatory input to the velocity integrator cells.

CBM cells. The model cerebellum is highly simplified. It channels sub-cortical SPEM information from NRTP and DLPN toward the vestibular nuclei which control the eye muscles. Hence, cerebelloctomy results in large and lasting deficits in pursuit (Zee, Yamazaki, Butler, & Gucer, 1981). The activities of these cells are given by:

$$\frac{dc^P_d}{dt} = -0.5c^P_d + (1 - c^P_d)\left(10\sum_v [p^D_{vd}]^+ + 20p^N_{vd}\right) - 25(1 + c^P_d)\sum_{e\neq d} c^P_e + 0.1c^P_d\Delta_N. \tag{24}$$

The cerebellum cell activities c^P_d are directionally tuned and receive excitatory input from DLPN ($\sum_v p^D_{vd}$) and NRTP (p^N_{vd}) from both hemispheres. Mutual inhibition occurs across directions ($-25\sum_{e\neq d} c^P_e$). Since cerebellum cells are velocity sensitive but not velocity tuned, the DLPN cell input is pooled over all velocities along a particular direction.

rLVN/MVN cells. Vestibular nuclei (medial and rostro-lateral vestibular nuclei) represent the penultimate stage of processing for SPEM. Here the directional representation is broken down from its cardinal axes into axes along which the muscle can move the eye. Since there are eight cardinal directions (d) represented by the model cerebellar pursuit cells and there are 4 orthogonal directions in which the muscle can move the model eye (represented by θ), the outputs from three cerebellum cells form one rLVN/MVN input. For example, the rLVN/MVN input along the upward direction ($\theta = 90°$), is defined by adding the cerebellar cells that are active for top-right ($d = 45°$), top ($d = 90°$), and top-left ($d = -45°$) directions:

$$I^P_\theta = c^P_{\theta-45°} + c^P_\theta + c^P_{\theta+45°}. \tag{25}$$

Pursuit neuron activities in the rLVN/MVN are defined by:

$$\frac{dh_\theta}{dt} = -0.6h_\theta + 4I^P_\theta - 1.5I^P_\Theta - 7.5v(o) + 0.1h_\theta\Delta_N. \tag{26}$$

By (26), these cells receive pursuit input ($4I^P_\theta$) from the cerebellum. They are inhibited by opponent direction pursuit input ($-1.5I^P_\Theta$) and by the omnipause neurons ($-v(o)$) in the brain stem. The signal function $v(x)$ is a sigmoid, calibrated such that inhibition from OPNs during pursuit is not enough to totally inhibit activity of pursuit neurons. It is given by:

$$v(x) = \frac{x^4}{x^4 + 0.5^4}. \tag{27}$$

During sustained pursuit, the inhibition from OPNs is high, but not strong enough to inhibit pursuit activity. During saccades, OPNs become silent and this causes the inhibition to become zero and helps pursuit neurons to reach the target velocity faster (post-saccadic enhancement of eye velocity, see Simulation 2). As above, direction θ takes the values of 0°, 90°, 180° and 270°, which represent rightward, upward, leftward and downward directions of motion. Parameter Θ in Eq. (26) is defined as: $\Theta = \theta + 180°$.

OPN cells. Omnipause neurons (OPNs) are tonically active cells present in the nucleus raphe interpositus and are known to inhibit saccades. They are active during periods of sustained pursuit and fixation, but become silent during saccades. The model OPN activities follow Gancarz and Grossberg (1999) and are defined as:

$$\frac{do}{dt} = -0.2o + (1 - o)(1.2 + 20[u_{ff}]^+) - 3.5(o + 0.4)(20v(l_\theta) + 5v(h_\theta)) + 0.1o\Delta_N. \tag{28}$$

Model OPNs are excited by an arousal signal (term 1.2) and SC fixation cell output (term u_{ff}, see Eq. (42)). These cells are inhibited by long lead burst neurons ($v(l_\theta)$, see Eq. (73)) as well as pursuit neurons ($v(h_\theta)$, see Eq. (26)), but by varying degrees. The sigmoidal signal function ($v(x)$) obeys:

$$v(x) = \frac{x^4}{x^4 + 0.1^4}. \tag{29}$$

The strength of inhibition from long lead burst neurons is stronger than pursuit neurons because OPNs go silent during saccades but are active at 66% of their maximal value during maintained pursuit (Missal & Keller, 2002).

SC cells. The model SC includes two cell layers or maps: SC burst cells and buildup cells (Munoz & Wurtz, 1993a, 1993b, 1995a, 1995b). SC receives collaterals from FEF, LIP and from LGN. Activities of these cells are represented by equations which are similar to equations in Gancarz and Grossberg (1999).

SC burst cells. Model SC burst cells represent the saccadic burst cells present in SC (Munoz & Wurtz, 1993a, 1993b, 1995a, 1995b). These have a burst of activity before a saccade and are quite silent during fixation and saccade preparation periods. Burst cell activities b_{ij} obey the equation:

$$\frac{db_{ij}}{dt} = -20b_{ij} + (1.2 - b_{ij})B^E_{ij} - (1 + b_{ij})B^I_{ij} + 0.1b_{ij}\Delta_N. \tag{30}$$

where the excitatory input equals:

$$B^E_{ij} = 8r_{ij} + 30f(u_{ij}) + 155.0[f^O_{ij}]^+. \tag{31}$$

SC burst cells receive excitatory input from the retina (r_{ij}), from buildup cells (u_{ij}, see Eq. (35)) and from the output layer of the FEF (f^O_{ij}, see Eq. (54)). The sigmoidal signal function ($f(u_{ij})$) is defined as:

$$f(x) = \frac{x^3}{x^3 + 0.07^3}. \tag{32}$$

The SC burst cell inhibitory input equals:

$$B^I_{ij} = 10M + 70[u_{ff}]^+ + 110n(n_{ij}). \tag{33}$$

These cells are inhibited by the mesencephalic reticular formation (M, see Eq. (46)), the fixation cell (u_{ff}, see Eq. (42)) and by the substantia nigra ($n(n_{ij})$, see Eq. (47)). The sigmoidal function ($n(x)$) is defined as:

$$n(x) = \frac{x^3}{x^3 + 0.4^3}. \tag{34}$$

SC buildup cells. Model buildup cells mimic the SC buildup cells in SC. They have no activity during fixation and show sustained buildup activity during the saccade preparation phase followed by a burst of activity prior to saccade initiation. The activities of the SC buildup cell layer (u_{ij}) obey the equation:

$$\frac{du_{ij}}{dt} = -0.1u_{ij} + (1 - u_{ij})U^E_{ij} - u_{ij}U^I_{ij} + 0.1u_{ij}\Delta_N. \tag{35}$$

The excitatory input to SC buildup cells (U^E_{ij}) is given by:

$$U^E_{ij} = r_{ij} + 5[f^I_{ij}]^+ + [a_{ij}]^+ + 40c(u_{ij}) + 4\sum_l\sum_k g(b_{lk}H_{k-j}H_{l-i}), \tag{36}$$

where

$$g(x) = 0.035x^{0.65}. \tag{37}$$

SC buildup cells are excited by the retina (r_{ij}), the planning layer of the FEF (f^I_{ij}, see Eq. (48)), the parietal cortex (a_{ij}, see Eq. (59)), and via self-excitatory connections ($c(u_{ij})$), by the burst cell layer (b_{lk}) and noise ($0.1u_{ij}\Delta_N$). The self-excitatory feedback signal is threshold-linear:

$$c(x) = [x - 0.035]^+. \tag{38}$$

The spread of input from the burst layer to buildup layer is a Gaussian described by:

$$H_i = 100e^{-i^2}. \tag{39}$$

The inhibitory input to SC buildup cells (U^I_{ij}) is given by:

$$U^I_{ij} = 40M + 0.8[u_{ff}]^+ + 8n(n_{ij}) + \sum_{\substack{l=j-6\\ l\neq j}}^{l=j+6} \sum_{\substack{k=i-6\\ k\neq i}}^{k=i+6} c(u_{kl})M_{k-i}M_{l-j}. \tag{40}$$

Inhibition comes from the mesencephalic formation (term M), the fixation cell (u_{ff}), the substantia nigra ($n(n_{ij})$), and other buildup cells ($c(u_{kl})$). There is strong mutual inhibition between buildup cells. The strength (M_i) of this inhibition is a Gaussian function of distance:

$$M_i = e^{-0.02i^2}. \tag{41}$$

SC fixation cells. Fixation cells are active during fixation and become silent during saccades. Model SC fixation cells obey:

$$\frac{du_{ff}}{dt} = -0.1u_{ff} + (0.1 - u_{ff})(10\zeta + r_{00} + K^E) - u_{ff}\left(10\sum_{\substack{k=1\\ k\neq f}}^{N}\sum_{\substack{j=1\\ j\neq f}}^{N} u_{kj}M_jM_k + 10\sum_{\substack{k=1\\ k\neq f}}^{N}\sum_{\substack{j=1\\ j\neq f}}^{N} b_{kj}\right) + 0.1u_{ff}\Delta_N. \tag{42}$$

The fixation cell activity (u_{ff}) is excited by a fixation signal (term ζ), defined as:

$$\zeta = \begin{cases} 1.0 & \text{if } t < T_{fix} (T_{fix} \\ & \text{is the time at which fixation light goes off}) \\ 0 & \text{otherwise.} \end{cases} \tag{43}$$

It is also excited by visual input from the fovea (r_{00}) and MT cells (K^E, see simulation 1) whose receptive fields contain the fovea, defined by:

$$K^E = \sum_{ij\in F_\delta} m^-_{ijvd} \quad \text{where}$$

$$F_\delta = \left\{ \begin{matrix} (i,j) \text{ such that } f-\delta \le i \le f+\delta \\ \text{and } f-\delta \le j \le f+\delta \end{matrix} \right\}. \tag{44}$$

In (44), δ is the radius of response field of the MT cell at position (i, j), and f indicates the position of the fovea.

Activity in buildup cells (term u_{kj}) or burst cells (term b_{kj}) inhibits fixation cell activity. As a result, once a saccade is initiated, fixation cells go silent. Since buildup layer cells are involved in saccade planning as well as saccade execution, both buildup and fixation cell activity can co-exist. This property is realized by using a distance-dependent Gaussian inhibition from buildup cells to fixation cells (term $10\sum_{k=2}^{N}\sum_{j=2}^{N} u_{kj}M_jM_k$). The buildup inhibitory kernel equals:

$$M_i = 0.1e^{-0.01i^2}. \tag{45}$$

MRF cells. The mesencephalic reticular formation input in Eqs. (33) and (40) is defined by:

$$M = \begin{cases} 1 & \text{if } \sum_{i,j\neq fovea}^{N} u_{ij} > 0 \\ 0 & \text{otherwise.} \end{cases} \tag{46}$$

It is active if there is any activity in the nonfoveal part of SC buildup cell layer (u_{ij}).

SNr cell. Cell activity (n_{ij}) in the model substantia nigra follows the equation:

$$\frac{dn_{ij}}{dt} = (1 - n_{ij})(1.7 + 200\zeta) - 2(1 + n_{ij})n(f^I_{ij}) + 0.1n_{ij}\Delta_N. \tag{47}$$

It is excited by a constant arousal signal (term 1.7) and by the fixation signal (ζ, see Eq. (43)). The nigral cells are inhibited by the FEF planning layer cells (f^I_{ij}, see Eq. (48)).

FEF cells: The model's frontal eye field is comprised of two cell layers or maps: FEF planning cells and output cells.

FEF planning layer cells. The FEF planning layer cells are involved in saccadic planning and execution. Reciprocal connections with LIP help these cells achieve target selection in a stimulus rich environment. The equations for planning cell activity f^I_{ij} at each position (i, j) is a simplified representation of a similar equation in Brown et al. (2004):

$$\frac{df^I_{ij}}{dt} = (1 - f^I_{ij})F^{PE}_{ij} - (f^I_{ij} + 0.4)F^{PI}_{ij} + 0.1f^I_{ij}\Delta_N \tag{48}$$

where the excitatory input (F^{PE}_{ij}) obeys:

$$F^{PE}_{ij} = 10[a_{ij}]^+ + 15I_{ij} + 1.5[g^S - 0.5]^+ + 2f(f^I_{ij}). \tag{49}$$

Each planning layer cell at position (i, j) receive excitatory input from the parietal cortex (a_{ij}), and from a smoothed retinal input (I_{ij}) defined as:

$$I_{ij} = \sum_{(p,q)\in\psi} R_{ij} \exp\left(\frac{-(p-i)^2 - (q-j)^2}{0.7^2}\right) \tag{50}$$

where Ψ is the set of eight nearest neighbors in cartesian input space. Additional excitatory input in Eq. (49) comes from the decision variable ($[g^S - 0.5]^+$) and via a self-excitatory recurrent on-center (term $2f(f^I_{ij})$). When the decision signal (g^s) goes over 0.5, it boosts the activity of all active neurons. This additional excitation gets amplified by the self-excitatory loop. That is, this combination ensures that the maximally active neuron gets the biggest boost in activity compared to the rest of the neurons. Thus, this combination realizes a target selection network among the planning layer neurons. The sigmoidal signal function ($f(x)$) controlling the FEF planning cell input is defined as:

$$f(x) = \frac{([x]^+)^8}{([x]^+)^8 + 0.5^8}. \tag{51}$$

The inhibitory input to Eq. (48) obeys:

$$F^{PI}_{ij} = 0.8 + 10([f^I_{ff}]^+ e^{-((i-f)^2+(j-f)^2)}) + 20\sum_{\substack{r\neq i\\ s\neq j}} f^I_{rs} + 10S_{on}. \tag{52}$$

In (52), each planning layer cell receives a distance-dependent inhibition from the FEF fixation cell (term f^I_{ff}), and from other active FEF planning cells via recurrent inhibition ($20\sum_{\substack{r\neq i\\ s\neq j}} f^I_{rs}$). These cells also get strong inhibition after saccade initiation in the form of "*saccade on*" signal (S_{on}). This signal takes the value 1 only if a saccade is underway and is zero during the rest of the interval. This might be thought of as FEF post-saccadic cell input.

FEF fixation cell. f_{ff}^I is the activity of the FEF fixation cell that is analogous to the SC fixation cell. It obeys the equation:

$$\frac{df_{ff}^I}{dt} = -0.1f_{ff}^I + (1 - f_{ff}^I)(10\varsigma + r_{00}) - (1 + f_{ff}^I)F_{ff}^I + 0.1f_{ff}^I \Delta_N. \tag{53}$$

This cell receives excitatory input from the fovea (r_{00}) and from the fixation input (ζ, described in Eq. (43)). The inhibitory input to the fixation cells obeys:

$$F_{ff}^I = 0.1 \sum_{ij} (f_{ij}^I e^{-0.01((i-f)^2+(j-f)^2)} + f_{ij}^O). \tag{54}$$

FEF fixation cells are inhibited by the FEF input cells (f_{ij}^I) and output cells (f_{ij}^O), much like the SC fixation cells.

FEF output cells. Model FEF output cells correspond to FEF movement or presaccadic cells. They convey the saccadic choice to SC and to the saccade generator in brain stem and thereby help execute a saccade. Their activities are defined by:

$$\frac{df_{ij}^O}{dt} = (1 - f_{ij}^O)F_{ij}^{OE} - (f_{ij}^O + 0.8)F_{ij}^{OI} + 0.1f_{ff}^O \Delta_N. \tag{55}$$

In (55), the excitatory input F_{ij}^{OE} obeys the equation:

$$F_{ij}^{OE} = 0.4[f_{ij}^I - 0.2]^+ + 5[a_{ij}]^+ + 1.5[g^S - 0.5]^+. \tag{56}$$

Excitatory inputs come from FEF input cells ($0.4[f_{ij}^I - 0.2]^+$) and parietal cells ($5a_{ij}$), but their suprathreshold activation strongly depends on excitation by the decision signal ($1.5[g^S - 0.5]^+$).

The inhibitory input F_{ij}^{OI} in Eq. (55) obeys:

$$F_{ij}^{OI} = 20 \sum_{\substack{p \neq i \\ q \neq j}} f_{pq}^O, \tag{57}$$

which provides strong mutual inhibition from other FEF output cells ($20 \sum_{\substack{p \neq i \\ q \neq j}} f_{pq}^O$). This strong mutual inhibition ensures that only the maximally active cell in the planning layer goes on to become a motor output, i.e., to generate a saccade.

Decision signal. The decision variable g^S, which is meant to represent the results of a competitive choice by a cortico-(basal ganglia)-thalamo–cortical loop (see in Brown et al. (2004)):

$$\frac{dg^S}{dt} = -0.6g^S + 20(1 - g^S)\left(\sum_{ij}([f_{ij}^I - 0.33]^+ + [a_{ij} - 0.6]^+ + [u_{ij} - 0.2]^+) + 0.1g^S \Delta_N\right). \tag{58}$$

In (58), activity g^S is maximal when there are synchronous inputs from all the three retinotopically in-register areas namely: FEF planning layer cells (f_{ij}^I), LIP visual cells (a_{ij}), and SC buildup cells (u_{ij}). Higher values of g^S enable faster target selection.

PPC cells. Parietal cortex cell activities (a_{ij}) represent the responses in the lateral bank of intra-parietal area (LIP), which code visual stimuli in motor error coordinates. They receive retinal and FEF input and project back to the FEF. They are modeled as:

$$\frac{da_{ij}}{dt} = (1 - a_{ij})[I_{ij} + [f_{ij}^I]^+ + f(f_{ij}^O) + f(a_{ij})] - a_{ij}\left[20 \sum_{\substack{x \neq i \\ y \neq j}} [a_{xy}]^+ + a_{ij}^R\right] + 0.1a_{ij}\Delta_N. \tag{59}$$

The excitatory input consists of a smoothed retinal input (I_{ij}, see Eq. (50)), FEF planning cells (f_{ij}^I), FEF output cells ($f(f_{ij}^O)$), and recurrent on-center connections ($f(a_{ij})$). The parameters for the sigmoidal signal function ($f(x)$, in Eq. (59)) were chosen such that there is sustained activity even during the delay period of the delayed-saccade paradigm. It is described as:

$$f(x) = \frac{x^7}{x^7 + 0.4^7}. \tag{60}$$

The inhibitory input to these cells consists of recurrent off-surround connections ($20 \sum_{\substack{x \neq i \\ y \neq j}} [a_{xy}]^+$) and a more slowly varying recurrent self-inhibition (a_{ij}^R, see Eq. (61)). Dynamics for the interneuron-mediated self-inhibition obey:

$$\frac{da_{ij}^R}{dt} = (1 - a_{ij}^R)a_{ij}^- - a_{ij}^R + 0.1a_{ij}^R \Delta_N. \tag{61}$$

These inhibitory connections replicate the slow decay of delay-period activity observed in primate parietal cells when the animal was doing a delayed saccade.

CBM cells: SC burst cells (b_{ij}) and FEF output cells (f_{ij}^O) activate cerebellar cells that control the learning of eye movement gains. The SC-activated cerebellar cell activities (c_{ij}^S) obey:

$$\frac{dc_{ij}^S}{dt} = -0.1c_{ij}^S + (1 - c_{ij}^S)r(b_{ij}) - 6(c_{ij}^S + 0.05) \times \sum_{i,j=1}^{N} o(c_{ij}^F) + 0.1c_{ij}^S \Delta_N. \tag{62}$$

Here, excitatory input comes from SC burst cells ($r(b_{ij})$) and inhibition from all cerebellar FEF-activated cells ($-\sum_{i,j=1}^{N} o(c_{ij}^F)$). Similarly, FEF-activated cells activities (c_{ij}^F) obey:

$$\frac{dc_{ij}^F}{dt} = -0.1c_{ij}^F + (1 - c_{ij}^F)r(f_{ij}^O) - (c_{ij}^F + 0.05) \times \sum_{i,j=1}^{N} o(c_{ij}^S) + 0.1c_{ij}^F \Delta_N. \tag{63}$$

These cells are excited by the output layer of FEF ($r(f_{ij}^O)$) and inhibited by all the cerebellar SC cells ($-\sum_{i,j=1}^{N} o(c_{ij}^S)$). The SC and FEF cerebellar cells hereby inhibit each other and compete for dominance (Gancarz & Grossberg, 1999). The excitatory signal function ($r(x)$, in Eqs. (62) and (63)) is defined by:

$$r(x) = \frac{x^4}{x^4 + 0.2^4}. \tag{64}$$

The inhibitory sigmoidal function ($o(x)$, in Eqs. (62) and (63)) given by:

$$o(x) = \frac{x^2}{x^2 + 0.5^2}. \tag{65}$$

Using the same excitatory and inhibitory sigmoidal functions for SC-activated and FEF-activated cerebellar cells biases the network such that FEF activity gets more preference if the maximal activities of FEF output cells and SC burst cells are out of sync. That is, the output saccade vector will not be a vector average, but will be more biased toward the vector represented by the maximally active FEF output cell.

Cerebellar learning corrects movement errors via adaptive gain control. For example, if the saccadic target was at position (10°, 10°) and the saccade landed the eye at (9°, 11°) from its original position, then the retinotopic error is (1°, −1°). The error

B_θ, where $\theta = 0°, 90°, 180°$, or $270°$, is calculated by breaking the retinotopic location into its constituent horizontal and vertical components. Thus the error takes the values: $B_{0°} = 1, B_{90°} = -1$, $B_{180°} = 0$ and $B_{270°} = 0$ when the eye foveates after moving 9° to right and 11° upwards. Learning is triggered in the cerebellum by the error-driven teaching signals γ_θ, and is given by:

$$\gamma_\theta = B_\theta. \tag{66}$$

The teaching signal is on for just a single integration step. The adaptive weights learn when both the teaching and the sampling signals are present. Opponent learning $(\gamma_\theta - \gamma_\Theta)$ allows weights to either increase or decrease and thus correct saccadic undershoots or overshoots (Grossberg & Kuperstein, 1986). The learning rules for weights mediating the FEF-activated cells (W^F_{ij}), SC-activated cerebellar cells (W^S_{ij}) and DLPN cells (W^D_{ij}) are given by:

$$\frac{dW^S_{ij}}{dt} = 67.5c^S_{ij}(\gamma_\theta - \gamma_\Theta), \tag{67}$$

$$\frac{dW^F_{ij}}{dt} = 67.5c^F_{ij}(\gamma_\theta - \gamma_\Theta), \tag{68}$$

$$\frac{dW^D_{vd}}{dt} = 67.5p^D_{vd}(\gamma_\theta - \gamma_\Theta). \tag{69}$$

PPRF cells: Equations defining saccade generator cell activities are similar to equations present in Gancarz and Grossberg (1999). The saccadic drive (I^S_θ) is calculated by adding direct SC input with the cerebellar input and is described by:

$$I^S_\theta = 120\left(\sum_{j=1}^{N}\sum_{i=1}^{N}(c^S_{ij}W^S_{ij} + c^F_{ij}W^F_{ij}) + \sum_d\sum_v p^D_{vd}W^D_{vd} + 4K^B + 4K^U\right). \tag{70}$$

Saccadic input from the cerebellum is the sum of all weighed activities of FEF (c^F_{ij}), SC(c^S_{ij}) and DLPN (p^D_{vd}) signals. The direct projections from the SC burst cells (K^B) and SC buildup layers (K^U) pass through sigmoidal transfer functions defined by Eqs. (71) and (72), respectively:

$$K^B = \frac{b^3_{ij}}{0.4^3 + b^3_{ij}} \tag{71}$$

and

$$K^U = \frac{u^3_{ij}}{0.1^3 + u^3_{ij}}. \tag{72}$$

The turning points (0.4 and 0.1) of the sigmoidal functions (K^B and K^U) were chosen so that, in case FEF is lesioned, there will be enough drive from SC to initiate a saccade.

Long lead burst cells (LLBNs): LLBNs form the input stage for the saccade generator. They receive input from cerebellum and SC. They provide accelerate and brake signals needed for saccade initiation and termination. The LLBN activities (l_θ) obey the equation:

$$\frac{dl_\theta}{dt} = -1.3l_\theta + I^S_\theta - 2I^S_\Theta - 2b_\theta. \tag{73}$$

In (73), Θ indicates the opposite direction and is defined as $\Theta = \theta + 180$.

The LLBN activity follows a push–pull opponent mechanism. It is excited by saccadic drive along its preferred direction (I^S_θ) and is inhibited by both the saccadic drive along the opponent direction ($2I^S_\Theta$) and by the inhibitory burst neurons (term $2b_\theta$, see Eq. (75)). Stronger coefficients for the inhibitory inputs ($2I^S_\Theta$ and $2b_\theta$, twice the excitatory input I^S_θ) are needed to achieve fast and accurate braking and thereby help in saccade termination.

Excitatory burst neurons (EBNs): EBNs receive input from LLBNs and are inhibited by the OPNs. As long as EBNs are active, the eye keeps moving. EBN cell activities (e_θ) are modeled as:

$$\frac{de_\theta}{dt} = -3.5e_\theta + (2 - e_\theta)(5l_\theta + 1) - (1 + e_\theta)(2l_\Theta + 20v(o)). \tag{74}$$

Excitatory input comes from the agonistic LLBNs (l_Θ) as well as an arousal signal (set equal to 1). Antagonistic LLBNs (l_Θ) and OPNs ($v(o)$, see Eq. (28)) inhibit the cell.

Inhibitory burst neurons (IBNs): IBN cell activities (b_θ) form a negative feedback loop that controls the amplitude and duration of LLBN activity. They obey the equation:

$$\frac{db_\theta}{dt} = -15b_\theta + 50e_\theta. \tag{75}$$

The Inhibitory burst neurons are excited by the agonistic EBNs (e_θ) and send inhibitory feedback to the agonistic LLBNs (l_θ, Eq. (73)).

Tonic neurons: Tonic neurons integrate the EBN burst (e_θ) and pursuit (h_θ) cell outputs via push–pull opponent organization:

$$\frac{dt_\theta}{dt} = 0.3(e_\theta - e_\Theta) + 0.15(h_\theta - h_\Theta). \tag{76}$$

Eye position (Ψ) is changed using the following formula:

$$\Psi = 20(t_\theta - t_\Theta). \tag{77}$$

Opponency ($t_\theta - t_\Theta$) allows the eye to change its direction smoothly while tracking a target which makes sudden changes in its direction of motion.

References

Albright, T. D. (1984). Direction and orientation selectivity of neurons in visual area MT of the macaque. *Journal of Neurophysiology*, *52*(6), 1106–1130.

Andersen, R. A., Asanuma, C., Essick, G., & Siegel, R. M. (1990). Corticocortical connections of anatomically and physiologically defined subdivisions within the inferior parietal lobule. *Journal of Comparative Neurology*, *296*(1), 65–113.

Arakawa, G. 2003. An adaptive model of smooth pursuit eye movements. Ph.D. Thesis. Boston University, Boston.

Barbas, H., & Mesulam, M. M. (1981). Organization of afferent input to subdivisions of area 8 in the rhesus monkey. *Journal of Comparative Neurology*, *200*(3), 407–431.

Basso, M. A., Krauzlis, R. J., & Wurtz, R. H. (2000). Activation and inactivation of rostral superior colliculus neurons during smooth-pursuit eye movements in monkeys. *Journal of Neurophysiology*, *84*(2), 892–908.

Basso, M. A., & Wurtz, R. H. (2002). Neuronal activity in substantia nigra pars reticulata during target selection. *Journal of Neuroscience*, *22*(5), 1883–1894.

Blatt, G. J., Andersen, R. A., & Stoner, G. R. (1990). Visual receptive field organization and cortico–cortical connections of the lateral intraparietal area area LIP in the macaque. *Journal of Comparative Neurology*, *299*(4), 421–445.

Blohm, G., Missal, M., & Lefèvre, P. (2003). Interaction between smooth anticipation and saccades during ocular orientation in darkness. *Journal of Neurophysiology*, *89*(3), 1423–1433.

Blohm, G., Missal, M., & Lefèvre, P. (2005). Direct evidence for a position input to the smooth pursuit system. *Journal of Neurophysiology*, *94*(1), 712–721.

Born, R. T., Groh, J. M. m., Zhao, R., & Lukasewycz, S. J. (2000). Segregation of object and background motion in visual area MT: effects of microstimulation on eye movements. *Neuron*, *26*, 725–734.

Born, R., & Tootell, R. (1992). Segregation of global and local motion processing in macaque middle temporal cortex. *Nature*, *357*, 497–499.

Brodal, P. (1980a). The cortical projection to the nucleus reticularis tegmenti pontis in the rhesus monkey. *Experimental Brain Research*, *38*(1), 19–27.

Brodal, P. (1980b). The projection from the nucleus reticularis tegmenti pontis to the cerebellum in the rhesus monkey. *Experimental Brain Research*, *38*(1), 29–36.

Brown, J. W., Bullock, D., & Grossberg, S. (2004). How laminar frontal cortex and basal ganglia circuits interact to control planned and reactive saccades. *Neural Network*, *17*(4), 471–510.

Buttner-Ennever, J. A., & Horn, A. K. (1997). Anatomical substrates of oculomotor control. *Current Opinion in Neurobiology*, *7*(6), 872–879.

Carpenter, G. A., & Grossberg, S. (1993). Normal and amnesic learning, recognition and memory by a neural model of cortico–hippocampal interactions. *Trends Neuroscience*, *16*(4), 131–137.

Chou, I. H., Sommer, M. A., & Schiller, P. H. (1999). Express averaging saccades in monkeys. *Vision Research*, *39*(25), 4200–4216.

Churchland, A. K., & Lisberger, S. G. (2005). Discharge properties of MST neurons that project to the frontal pursuit area in macaque monkeys. *Journal of Neurophysiology*, *94*(2), 1084–1090.

Collins, C. E., Lyon, D. C., & Kaas, J. H. (2005). Distribution across cortical areas of neurons projecting to the superior colliculus in new world monkeys. *Anat Rec A Discov Mol Cell Evol Biol*, *285*(1), 619–627.

Davidson, R. M., & Bender, D. B. (1991). Selectivity for relative motion in the monkey superior colliculus. *Journal of Neurophysiology*, *65*(5), 1115–1133.

de Brouwer, S., Missal, M., & Lefèvre, P. (2001). Role of retinal slip in the prediction of target motion during smooth and saccadic pursuit. *Journal of Neurophysiology*, *86*(2), 550–558.

de Brouwer, S., Yuksel, D., Blohm, G., Missal, M., & Lefèvre, P. (2002). What triggers catch-up saccades during visual tracking? *Journal of Neurophysiology*, *87*(3), 1646–1650.

de Brouwer, S., Missal, M., Barnes, G., & Lefèvre, P. (2002). Quantitative analysis of catch-up saccades during sustained pursuit. *Journal of Neurophysiology*, *87*(4), 1772–1780.

Dominey, P. F., & Arbib, M. A. (1992). A cortico-subcortical model for generation of spatially accurate sequential saccades. *Cereb Cortex*, *2*(2), 153–175.

Droulez, J., & Berthoz, A. (1991). A neural network model of sensoritopic maps with predictive short-term memory properties. *Proceedings of the National Academy of Sciences of the USA*, *88*(21), 9653–9657.

Eggert, T., Guan, Y., Bayer, O., & Buttner, U. (2005). Saccades to moving targets. *Annals of the New York Academy of Sciences*, *1039*, 149–159.

Everling, S., Pare, M., Dorris, M. C., & Munoz, D. P. (1998). Comparison of the discharge characteristics of brain stem omnipause neurons and superior colliculus fixation neurons in monkey: implications for control of fixation and saccade behavior. *Journal of Neurophysiology*, *79*(2), 511–528.

Fries, W. (1984). Cortical projections to the superior colliculus in the macaque monkey: a retrograde study using horseradish peroxidase. *Journal of Comparative Neurology*, *230*(1), 55–76.

Gancarz, G., & Grossberg, S. (1999). A neural model of saccadic eye movement control explains task-specific adaptation. *Vision Research*, *39*(18), 3123–3143.

Gandhi, N. J., & Keller, E. L. (1997). Spatial distribution and discharge characteristics of superior colliculus neurons antidromically activated from the omnipause region in monkey. *Journal of Neurophysiology*, *78*(4), 2221–2225.

Gellman, R. S., & Fletcher, W. A. (1992). Eye position signals in human saccadic processing. *Experimental Brain Research*, *89*(2), 425–434.

Giolli, R. A., Gregory, K. M., Suzuki, D. A., Blanks, R. H., Lui, F., & Betelak, K. F. (2001). Cortical and subcortical afferents to the nucleus reticularis tegmenti pontis and basal pontine nuclei in the macaque monkey. *Vision Neuroscience*, *18*(5), 725–740.

Girad, B., & Berthoz, A. (2005). From brainstem to cortex: computational models of saccade generation circuitry. *Progress in Neurobiology*, *77*(4), 215–251.

Glickstein, M., Cohen, J. L., Dixon, B., Gibson, A., Hollins, M., Labossiere, E., et al. (1980). Corticopontine visual projections in macaque monkeys. *Journal of Comparative Neurology*, *190*(2), 209–229.

Gottlieb, J. P., Bruce, C. J., & MacAvoy, M. G. (1993). Smooth eye movements elicited by microstimulation in the primate frontal eye field. *Journal of Neurophysiology*, *69*(3), 786–799.

Grossberg, S. (1973). Contour enhancement, short-term memory, and constancies in reverberating neural networks. *Studies in Applied Mathematics*, *52*, 213–257.

Grossberg, S. (1980). Biological competition: decision rules, pattern formation, and oscillations. *Proceedings of the National Academy of Sciences of the USA*, *77*(4), 2338–2342.

Grossberg, S. (1982). *Studies of mind and brain*. Amsterdam: Kluwer/Reidel.

Grossberg, S. (2000). The complementary brain: unifying brain dynamics and modularity. *Trends Cognosy Science*, *4*(6), 233–246.

Grossberg, S. 2003. How does the cerebral cortex work? Development, Learning, Attention, and 3-D Vision by Laminar Circuits of Visual Cortex vol. 2, (pp. 47–76).

Grossberg, S., & Kuperstein, M. 1986. Neural dynamics of adaptive sensory-motor control: ballistic eye movements. Amsterdam: New York.

Grossberg, S., & Kuperstein, M. (1989). *Neural dynamics of adaptive sensory-motor control: expanded edition*. Elmsford, NY: Pergamon Press.

Grossberg, S., Mingolla, E., & Pack, C. (1999). A neural model of motion processing and visual navigation by cortical area MST. *Cereb Cortex*, *9*(8), 878–895.

Grossberg, S., Roberts, K., Aguilar, M., & Bullock, D. (1997). A neural model of multimodal adaptive saccadic eye movement control by superior colliculus. *Journal of Neuroscience*, *17*(24), 9706–9725.

Guan, Y., Eggert, T., Bayer, O., & Buttner, U. (2005). Saccades to stationary and moving targets differ in the monkey. *Experimental Brain Research*, *161*(2), 220–232.

Harting, J. K. (1977). Descending pathways from the superior collicullus: an autoradiographic analysis in the rhesus monkey Macaca mulatta. *Journal of Comparative Neurology*, *173*(3), 583–612.

Hodgkin, A. L. (1964). The ionic basis of nervous conduction. *Science*, *145*, 1148–1154.

Huerta, M. F., Krubitzer, L. A., & Kaas, J. H. (1987). Frontal eye field as defined by intracortical microstimulation in squirrel monkeys, owl monkeys, and macaque monkeys. II, cortical connections. *Journal of Comparative Neurology*, *265*(3), 332–361.

Jurgens, R., Becker, W., & Kornhuber, H. H. (1981). Natural and drug-induced variations of velocity and duration of human saccadic eye movements: evidence for a control of the neural pulse generator by local feedback. *Biological Cybernetics*, *39*(2), 87–96.

Kalesnykas, R. P., & Hallett, P. E. (1994). Retinal eccentricity and the latency of eye saccades. *Vision Research*, *34*(4), 517–531.

Kalesnykas, R. P., & Hallett, P. E. (1996). Fixation conditions, the foveola and saccadic latency. *Vision Research*, *36*(19), 3195–3203.

Keller, E. L., Gandhi, N. J., & Weir, P. T. (1996). Discharge of superior collicular neurons during saccades made to moving targets. *Journal of Neurophysiology*, *76*(5), 3573–3577.

Keller, E. L., & Khan, N. S. (1986). Smooth-pursuit initiation in the presence of a textured background in monkey. *Vision Research*, *26*(6), 943–955.

Kimmig, H. G., Miles, F. A., & Schwarz, U (1992). Effects of stationary textured backgrounds on the initiation of pursuit eye movements in monkeys. *Journal of Neurophysiology*, *68*, 2147–2164.

Klingstone, A., & Klein, R. (1991). Combining Shape and position expectancies: hierarchical processing and selective inhibition. *Journal of Experimental Psychology. Human Perception and Performance*, *17*(2), 512–519.

Kodaka, Y., Miura, K., Suehiro, K., Takemura, A., & Kawano, K (2003). Ocular tracking of moving targets: effects of perturbing the background. *Journal of Neurophysiology*, *91*, 2474–2483.

Krauzlis, R. J., Basso, M. A., & Wurtz, R. H. (2000). Discharge properties of neurons in the rostral superior colliculus of the monkey during smooth-pursuit eye movements. *Journal of Neurophysiology*, *84*(2), 876–891.

Krauzlis, R. J., & Miles, F. A. (1996a). Initiation of saccades during fixation or pursuit: evidence in humans for a single mechanism. *Journal of Neurophysiology*, *76*(6), 4175–4179.

Krauzlis, R. J., & Miles, F. A. (1996b). Transitions between pursuit eye movements and fixation in the monkey: dependence on context. *Journal of Neurophysiology*, *76*(3), 1622–1638.

Krauzlis, R. J. (2004). Recasting the smooth pursuit eye movement system. *Journal of Neurophysiology*, *91*(2), 591–603.

Krauzlis, R. J. (2005). The control of voluntary eye movements: new perspectives. *Neuroscientist*, *11*(2), 124–137.

Langer, T. P., & Kaneko, C. R. (1990). Brainstem afferents to the oculomotor omnipause neurons in monkey. *Journal of Comparative Neurology*, *295*(3), 413–427.

Lee, W. J., & Galiana, H. L. (2005). An internally switched model of ocular tracking with prediction. *IEEE Transactions on Neural Systems and Rehabilitaion Engineering*, *13*(2), 186–193.

Lefèvre, P., Quaia, C., & Optican, L. M. (1998). Distributed model of control of saccades by superior colliculus and cerebellum. *Neural Network*, *11*(7–8), 1175–1190.

Leichnetz, G. R. (1981). The prefrontal cortico-oculomotor trajectories in the monkey. *Journal of the Neurological Sciences*, *49*(3), 387–396.

Leichnetz, G. R., Smith, D. J., & Spencer, R. F. (1984). Cortical projections to the paramedian tegmental and basilar pons in the monkey. *Journal of Comparative Neurology*, *228*(3), 388–408.

Leichnetz, G. R., Spencer, R. F., Hardy, S. G., & Astruc, J. (1981). The prefrontal corticotectal projection in the monkey; an anterograde and retrograde horseradish peroxidase study. *Neuroscience*, *6*(6), 1023–1041.

Leigh, R. J., & Zee, D. S. (1999). *The neurology of eye movements* (3rd ed.). Oxford University Press.

Lindner, A., Schwarz, U., & Ilg, U. J (2001). Cancellation of self-induced retinal image motion during smooth pursuit eye movements. *Vision Research*, *41*, 1685–1694.

Lisberger, S. G. (1998). Postsaccadic enhancement of initiation of smooth pursuit eye movements in monkeys. *Journal of Neurophysiology*, *79*(4), 1918–1930.

Lisberger, S. G., Pavelko, T. A., & Broussard, D. M. (1994). Responses during eye movements of brain stem neurons that receive monosynaptic inhibition from the flocculus and ventral paraflocculus in monkeys. *Journal of Neurophysiology*, *72*(2), 909–927.

Lisberger, S. G., & Westbrook, L. E. (1985). Properties of visual inputs that initiate horizontal smooth pursuit eye movements in monkeys. *Journal of Neuroscience*, *5*, 1662–1673.

Lynch, J. C., Graybiel, A. M., & Lobeck, L. J. (1985). The differential projection of two cytoarchitectonic subregions of the inferior parietal lobule of macaque upon the deep layers of the superior colliculus. *Journal of Comparative Neurology*, *235*(2), 241–254.

Maioli, M. G., Domeniconi, R., Squatrito, S., & Riva Sanseverino, E. (1992). Projections from cortical visual areas of the superior temporal sulcus to the superior colliculus, in macaque monkeys. *Archive Italian Biology*, *130*(3), 157–166.

Masson, G., Proteau, L, & Mestre, D. R. (1995). Effects of stationary and moving textured backgrounds on the visuo-oculo-manual tracking in humans. *Vision Research*, *35*, 837–852.

Maunsell, J. H., & Van Essen, D. C. (1983). Functional properties of neurons in middle temporal visual area of the macaque monkey. I, selectivity for stimulus direction, speed, and orientation. *Journal of Neurophysiology*, *49*(5), 1127–1147.

May, P. J., & Porter, J. D. (1992). The laminar distribution of macaque tectobulbar and tectospinal neurons. *Vision Neuroscience*, *8*(3), 257–276.

McKenzie, A., & Lisberger, S. G. (1986). Properties of signals that determine the amplitude and direction of saccadic eye movements in monkeys. *Journal of Neurophysiology*, *56*(1), 196–207.

Missal, M., Coimbra, A., Lefèvre, P., & Olivier, E. (2002). Further evidence that a shared efferent collicular pathway drives separate circuits for smooth eye movements and saccades. *Experimental Brain Research*, *147*(3), 344–352.

Missal, M., & Keller, E. L. (2002). Common inhibitory mechanism for saccades and smooth-pursuit eye movements. *Journal of Neurophysiology*, *88*(4), 1880–1892.

Mohrmann, H., & Thier, P. (1995). The influence of structured visual backgrounds on smooth-pursuit initiation, steady-state pursuit and smooth-pursuit termination. *Biological Cybernetics*, *73*, 83–93.

Munoz, D. P., & Wurtz, R. H. (1993a). Fixation cells in monkey superior colliculus. I, characteristics of cell discharge. *Journal of Neurophysiology*, *70*(2), 559–575.
Munoz, D. P., & Wurtz, R. H. (1993b). Fixation cells in monkey superior colliculus. II, reversible activation and deactivation. *Journal of Neurophysiology*, *70*(2), 576–589.
Munoz, D. P., & Wurtz, R. H. (1995a). Saccade-related activity in monkey superior colliculus. I, characteristics of burst and buildup cells. *Journal of Neurophysiology*, *73*(6), 2313–2333.
Munoz, D. P., & Wurtz, R. H. (1995b). Saccade-related activity in monkey superior colliculus. II, spread of activity during saccades. *Journal of Neurophysiology*, *73*(6), 2334–2348.
Munoz, D. P., Dorris, M. C., Paré, M., & Everling, S. (2000). On your mark, get set: brainstem circuitry underlying saccadic initiation. *Canadian Journal of Physiology and Pharmacology*, *78*(11), 934–944.
Mustari, M. J., Fuchs, A. F., & Wallman, J. (1988). Response properties of dorsolateral pontine units during smooth pursuit in the rhesus macaque. *Journal of Neurophysiology*, *60*(2), 664–686.
Nagao, S., Kitamura, T., Nakamura, N., Hiramatsu, T., & Yamada, J. (1997). Differences of the primate flocculus and ventral paraflocculus in the mossy and climbing fiber input organization. *Journal of Comparative Neurology*, *382*(4), 480–498.
Newsome, W. T., Wurtz, R. H., & Komatsu, H. (1988). Relation of cortical areas MT and MST to pursuit eye movements. II, differentiation of retinal from extraretinal inputs. *Journal of Neurophysiology*, *60*(2), 604–620.
Niemann, T., & Hoffmann, K. P. (1997). The influence of stationary and moving textured backgrounds on smooth-pursuit initiation and steady state pursuit in humans. *Experimental Brain Research*, *115*, 531–540.
Ono, S., Das, V. E., Economides, J. R., & Mustari, M. J. (2005). Modeling of smooth pursuit-related neuronal responses in the DLPN and NRTP of the rhesus macaque. *Journal of Neurophysiology*, *93*(1), 108–116.
Ono, S., Das, V. E., & Mustari, M. J. (2004). Gaze-related response properties of DLPN and NRTP neurons in the rhesus macaque. *Journal of Neurophysiology*, *91*(6), 2484–2500.
Optican, L. M., & Quaia, C. (2002). Distributed model of collicular and cerebellar function during saccades. *Annals of the New York Academy of Sciences*, *956*, 164–177.
Orban de Xivry, J. J., & Lefèvre, P. (2007). Saccades and pursuit: two outcomes of a single sensorimotor process. *Journal of Physiology*, *584*(1), 11–23.
Pack, C., Grossberg, S., & Mingolla, E. (1998). Cortical processing of visual motion for smooth pursuit eye movements. *Society Neuroscience Abstract*, *24*, 3440.
Pack, C., Grossberg, S., & Mingolla, E. (2001). A neural model of smooth pursuit control and motion perception by cortical area MST. *Journal of Cogn Neuroscience*, *13*(1), 102–120.
Pare, M., & Guitton, D. (1994). The fixation area of the cat superior colliculus: effects of electrical stimulation and direct connection with brainstem omnipause neurons. *Experimental Brain Research*, *101*(1), 109–122.
Quaia, C., Lefèvre, P., & Optican, L. M. (1999). Model of the control of saccades by superior colliculus and cerebellum. *Journal of Neurophysiology*, *82*(2), 999–1018.
Rashbass, C. (1961). The relationship between saccadic and smooth tracking eye movements. *Journal of Physiology*, *159*, 326–338.
Robinson, D. A. (1964). The mechanics of human saccadic eye movement. *Journal of Physiology (London)*, *174*, 245–264.
Robinson, D. A., Gordon, J. L., & Gordon, S. E. (1986). A model of the smooth pursuit eye movement system. *Biological Cybernetics*, *55*(1), 43–57.
Roy, J. E., & Cullen, K. E. (2003). Brain stem pursuit pathways: dissociating visual, vestibular, and proprioceptive inputs during combined eye–head gaze tracking. *Journal of Neurophysiology*, *90*(1), 271–290.
Schreiber, C., Missal, M., & Lefèvre, P. (2006). Asynchrony between position and motion signals in the saccadic system. *Journal of Neurophysiology*, *95*(2), 960–969.
Scudder, C. A., Moschovakis, A. K., Karabelas, A. B., & Highstein, S. M. (1996a). Anatomy and physiology of saccadic long-lead burst neurons recorded in the alert squirrel monkey. I, descending projections from the mesencephalon. *Journal of Neurophysiology*, *76*(1), 332–352.
Scudder, C. A., Moschovakis, A. K., Karabelas, A. B., & Highstein, S. M. (1996b). Anatomy and physiology of saccadic long-lead burst neurons recorded in the alert squirrel monkey. II, pontine neurons. *Journal of Neurophysiology*, *76*(1), 353–370.
Seidemann, E., & Newsome, W. T. (1999). Effect of spatial attention on the responses of area MT neurons. *Journal of Neurophysiology*, *81*(4), 1783–1794.
Spatz, W. B., & Tigges, J. (1973). Studies on the visual area MT in primates. II, projection fibers to subcortical structures. *Brain Research*, *61*, 374–378.
Srihasam, K., Bullock, D., & Grossberg, S. (2005). Brain mechanisms for effective coordination of saccades and smooth pursuit eye movements during visual tracking and perception. *In Abstracts of the Society for Neuroscience (SFN)*, Washington, DC, No: 822.1 (Talk).
Srihasam, K., Bullock, D., & Grossberg, S. (2006a). Coordinating saccades and smooth pursuit eye movements during visual tracking and perception of objects moving with variable speeds (Abstract). *Journal of Vision*, *6*(6), 908.
Srihasam, K., Bullock, D., & Grossberg, S. (2006b). Network Computations For Intelligent Coordination Of Saccades And Smooth Pursuit Eye Movements During Tracking And Visual Perception. *In Abstracts of the Society for Neuroscience (SFN)*, Atlanta, GA.
Srihasam, K., Bullock, D., & Grossberg, S. (2007). Coordination of saccadic and smooth pursuit eye movements during target selection and tracking. *In Abstracts of the Society for Neuroscience (SFN)*, San Diego CA, November.
Srihasam, K., Bullock, D., & Grossberg, S. (2009). Target selection by the frontal cortex during coordinated saccadic and smooth pursuit eye movements. *Journal of Cognitive Neuroscience*, *21*(8), 1611–1627.
Suzuki, D. A., & Keller, E. L. (1984). Visual signals in the dorsolateral pontine nucleus of the alert monkey: their relationship to smooth-pursuit eye movements. *Experimental Brain Research*, *53*(2), 473–478.
Suzuki, D. A., Yamada, T., Hoedema, R., & Yee, R. D. (1999). Smooth-pursuit eye-movement deficits with chemical lesions in macaque nucleus reticularis tegmenti pontis. *Journal of Neurophysiology*, *82*(3), 1178–1186.
Suzuki, D. A., Yamada, T., & Yee, R. D. (2003). Smooth-pursuit eye-movement-related neuronal activity in macaque nucleus reticularis tegmenti pontis. *Journal of Neurophysiology*, *89*(4), 2146–2158.
Takagi, M., Zee, D. S., & Tamargo, R. J. (1998). Effects of lesions of the oculomotor vermis on eye movements in primate: saccades. *Journal of Neurophysiology*, *80*(4), 1911–1931.
Tam, W. J., & Stelmach, L. B. (1993). Viewing behavior: ocular and attentional disengagement. *Perception & Psychophysics*, *54*(2), 211–222.
Tanaka, K., Sugita, Y., Moriya, M., & Saito, H. (1993). Analysis of object motion in the ventral part of the medial superior temporal area of the macaque visual cortex. *Journal of Neurophysiology*, *69*(1), 128–142.
Tanaka, M., & Lisberger, S. G. (2002a). Enhancement of multiple components of pursuit eye movement by microstimulation in the arcuate frontal pursuit area in monkeys. *Journal of Neurophysiology*, *87*(2), 802–818.
Tanaka, M., & Lisberger, S. G. (2002b). Role of arcuate frontal cortex of monkeys in smooth pursuit eye movements. I, basic response properties to retinal image motion and position. *Journal of Neurophysiology*, *87*(6), 2684–2699.
Tanaka, M., Yoshida, T., & Fukushima, K. (1998). Latency of saccades during smooth-pursuit eye movement in man, directional asymmetries. *Experimental Brain Research*, *121*(1), 92–98.
Thielert, C. D., & Thier, P. (1993). Patterns of projections from the pontine nuclei and the nucleus reticularis tegmenti pontis to the posterior vermis in the rhesus monkey: a study using retrograde tracers. *Journal of Comparative Neurology*, *337*(1), 113–126.
Thier, P., & Ilg, U. J. (2005). The neural basis of smooth-pursuit eye movements. *Current Opinion in Neurobiology*, *15*(6), 645–652.
Tian,, & Lynch, J. C. (1997). Subcortical input to the smooth and saccadic eye movement subregions of the frontal eye field in Cebus monkey. *Journal of Neuroscience*, *17*(23), 9233–9247.
Tian, J. R., & Lynch, J. C. (1996a). Corticocortical input to the smooth and saccadic eye movement subregions of the frontal eye field in Cebus monkeys. *Journal of Neurophysiology*, *76*(4), 2754–2771.
Tian, J. R., & Lynch, J. C. (1996b). Functionally defined smooth and saccadic eye movement subregions in the frontal eye field of Cebus monkeys. *Journal of Neurophysiology*, *76*(4), 2740–2753.
Torigoe, Y., Blanks, R. H. I., & Precht, W. (1986). Anatomical studies on the nucleus reticularis tegmenti pontis in the pigmented rat. II, subcortical afferents demonstrated by the retrograde transport of horseradish peroxidase. *The Journal of Comparative Neurology*, *243*(1), 88–105.
Treue, S., & Maunsell, J. H. (1999). Effects of attention on the processing of motion in macaque middle temporal and medial superior temporal visual cortical areas. *Journal of Neuroscience*, *19*(17), 7591–7602.
Tusa, R. J., & Ungerleider, L. G. (1988). Fiber pathways of cortical areas mediating smooth pursuit eye movements in monkeys. *Annals of Neurology*, *23*(2), 174–183.
van den Berg, A. ,V., & Collewijn, H. (1986). Human smooth pursuit: effects of stimulus extent and of spatial and temporal constraints of the pursuit trajectory. *Vision Research*, *26*(8), 1209–1222.
Van Donkelaar, P., & Drew, A. S. (2002). The allocation of attention during smooth pursuit eye movements. *Progress of Brain Research*, *140*, 267–277.
Van Gelder, P., Lebedev, S., & Tsui, W. H. (1995). Predictive human pursuit and orbital goal of microstimulated smooth eye movements. *Journal of Neurophysiology*, *74*(3), 1358–1361.
Van Gelder, P., Lebedev, S., & Tsui, W. H. (1997). Peak velocities of visually and nonvisually guided saccades in smooth-pursuit and saccadic tasks. *Experimental Brain Research*, *116*(2), 201–215.
Waitzman, D. M., Ma, T. P., Optican, L. M., & Wurtz, R. H. (1991). Superior colliculus neurons mediate the dynamic characteristics of saccades. *Journal of Neurophysiology*, *66*(5), 1716–1737.
White, J. M., Sparks, D. L., & Stanford, T. R. (1994). Saccades to remembered target locations: an analysis of systematic and variable errors. *Vision Research*, *34*, 79–92.
Wurtz, R., Komatsu, H., Dursteler, M., & Yamasaki, D. (1990). Motion to movement: cerebral cortical processing for pursuit eye movements. In G. Edelman, & W. M. Cowen (Eds.), *Signal and sense: local and global order in perceptual maps* (pp. 233–260). New York: John Wiley.
Yamada, J., & Noda, H. (1987). Afferent and efferent connections of the oculomotor cerebellar vermis in the macaque monkey. *Journal of Comparative Neurology*, *265*(2), 224–241.
Yamada, T., Suzuki, D. A., & Yee, R. D. (1996). Smooth pursuitlike eye movements evoked by microstimulation in macaque nucleus reticularis tegmenti pontis. *Journal of Neurophysiology*, *76*(5), 3313–3324.
Yee, R. D., Daniels, S. A., Jones, O. W., Baloh, R. W., & Honrubia, V. (1983). Effects of an optokinetic background on pursuit eye movements. *Investigational Ophthalmol Vision Science*, *24*, 1115–1122.
Zee, D. S., Yamazaki, A., Butler, P. H., & Gucer, G. (1981). Effects of ablation of flocculus and paraflocculus of eye movements in primate. *Journal of Neurophysiology*, *46*(4), 878–899.